Materials Today Bio 12 (2021) 100138

Contents lists available at ScienceDirect

Materials Today Bio

journal homepage: www.journals.elsevier.com/materials-today-bio

A mechanical, electrical dual autonomous self-healing multifunctional composite hydrogel

Y. Wang [a], Y. Jia [a,b], H. Ren [a], C. Lao [a], W. Peng [c], B. Feng [a], J. Wang [a,*]

[a] Key Laboratory of Advanced Technologies of materials, Ministry of Education, School of Materials Science and Engineering, Southwest Jiaotong University, Chengdu, 610031, China
[b] Department of Electromechanical Engineering, Sichuan Engineering Technical College, Deyang, Sichuan, 618000, China
[c] Department of Biochemistry and Molecular Biology, College of Basic and Forensic Medicine, Sichuan University, Chengdu, 610041, China

ARTICLE INFO

Keywords:
Dual autonomous self-healing
Hydrogels
Multifunctional
Wound repair
Wearable strain sensors

ABSTRACT

The versatile properties make hydrogels a potential multipurpose material that finds wide applications. However, the preparation of multipurpose hydrogels is very challenging. Here, we report a method based on free radical reaction and composite mechanisms to prepare mechanical and electrical self-healing multifunctional hydrogels. In this study, the introduction of imidazolium salt ionic liquids and glycerol in the hydrogel system endows the gels with good antibacterial, conductive, and adhesive properties and excellent antifreeze properties. The testing results show that the as-prepared hydrogel has stable mechanical and electrical properties even under the extremely cold condition of −50°C after self-healing. Moreover, the active esters formed in the dynamic radical reaction have better reducibility, thus further investing the as-prepared hydrogel with high antioxidant activity. The application results show that these comprehensive properties make such hydrogel system very useful in wound repair and wearable strain sensors.

1. Introduction

It is well known that hydrogel is a complex multifunctional three-dimensional network structure. Owing to its high water content and its similarity with cell matrix, many good biocompatible hydrogels have been used in wound repair, cartilage replacement [1–3], cell culture scaffolds, and tissue engineering [4]. At present, the development of hydrogel with strong tissue adhesion, rapid electrical, and mechanical self-healing without external stimulation, good anti-freezing, antibacterial, antioxidant, mechanical, and conductive properties, which will be expected to achieve a wide range of biomedical applications, has become one of the main research directions of hydrogels in the future [5,6]. This also makes its research very challenging. Conductive hydrogels have similar structure to extracellular matrix and good biocompatibility and their network structure, physical, and mechanical properties and biological functions can be flexibly adjusted according to requirements and thus have unique advantages in biosensing organs and organs. Among these conductive hydrogels, ionic conductive hydrogel is considered as an ideal implantable sensor material. Its modulus and electrochemical properties are close to biological tissue. In addition, it has good flexibility, which is conducive to close adhesion with target tissues and organs and reducing interface impedance [7–9]. Therefore, it has been widely studied. Our present work would focus on the research of multifunctional conductive hydrogel. Although many multifunctional hydrogels have been achieved through various approaches, such hydrogel that has so many complex properties in one has rarely been reported [10–13], which means the more functions, the more materials involved, and the more complex the material system. How to gain more functions with less materials is a real tough issue.

Among so many functions, it is the most difficult to realize to achieve both mechanical and electrical self-healing properties. It is well known that if without good mechanical self-healing properties, it is impossible to achieve final stable electrical self-healing, while the selection of conductive mechanism plays a crucial role in achieving such duel self-healing property. In our previous study, we proposed the dynamic-free radical coupling reaction between tyramine hydrochloride (Tyr) catalyzed by non-enzymatic catalysis and obtained a strong reversible covalent bond and constructed a hydrogel (polyglutamic acid-tyramine hydrochloride hydrogel, PGA-Tyr hydrogel), which can autonomously self-heal at room temperature, for the first time. It laid the foundation for our design of hydrogel with mechanical self-healing and electrical self-healing properties and electrical and mechanical dual network

* Corresponding author.
E-mail address: jwang@swjtu.edu.cn (J. Wang).

https://doi.org/10.1016/j.mtbio.2021.100138
Received 25 July 2021; Received in revised form 2 September 2021; Accepted 5 September 2021
Available online 11 September 2021

structure. Such hydrogel system also presents good antioxidant properties because of the existence of dynamic radical reactions. On this basis, to endow such hydrogel system with good conductive and antibacterial properties, one imidazolium salt ionic liquid (IL) that has intrinsic antibacterial and conductive properties would be specially selected to be introduced into the hydrogel system [14,15]. In addition, in the help of strong hydrogen bond interaction that three hydrogen protons on the imidazole ring form with water molecules, some of the 'free water' can be converted to hydrated ions with higher binding energy [16], which can lead to the reduction of the freezing point and thus endow hydrogel with a certain degree of anti-freezing properties. Although IL has been reported to be used for the synthesis of ionic conductive hydrogel, such subtle consideration that can allow IL to realize multiple functions at the same time has not been reported. As we know, conductive hydrogels can be obtained in three ways [17]: (1) by introducing metal nanowires, carbon nanotubes, and graphene and other conductive fillers into hydrogels; (2) through the formation of conductive polymer network, which can be prepared via in-situ polymerization in hydrogels; (3) by introducing a better compatible ionic conductive phase, such as IL, into hydrogels. Compared with other methods, because of the unique properties of ILs, such as hydrophilicity and hydration capacity, the use of IL can be more beneficial for the formation of uniform and stable conductive network as the second network in hydrogel system. As a result, once mechanical self-healing is achieved, electrical self-healing is also achieved. This consideration has not been reported. Furthermore, we would introduce antifreeze agent glycerol rich in hydroxyl into the hydrogel to further enhance the adhesion and self-healing properties of the system [18] and endow the system with excellent antifreeze and service performance under extremely cold conditions. This kind of hydrogel with good self-healing, conductivity, antibacterial, freezing resistance, mechanical properties, antioxidant properties, adhesion, and biocompatibility will be expected to be applied not only as wound dressing to promote wound healing but also as a wearable strain sensor in health monitoring, human-computer interaction, and robot fields (Fig. 1).

2. Materials and methods

2.1. Materials

γ-PGA (weight-average molecular weight 1000 KDa) was purchased from Xi'an Bella Biotechnology Co., Ltd. (Xi'an, China). Tyramine hydrochloride (Tyr·HCl), 1-(3-dimethylaminopropyl)-3-ethyl-carbodiimide (EDC·HCl, ≥98.0%), and 1-hydroxypyrrolidine (NHS, ≥98.0%) were purchased from Shanghai Macklin Biochemical Co., Ltd. (Shanghai, China). Glycerol and 1-butyl-3-methylimidazolium tetrafluoroborate ([BMIM][BF_4], ≥99.0%) were obtained from Kelong Chemical Reagent

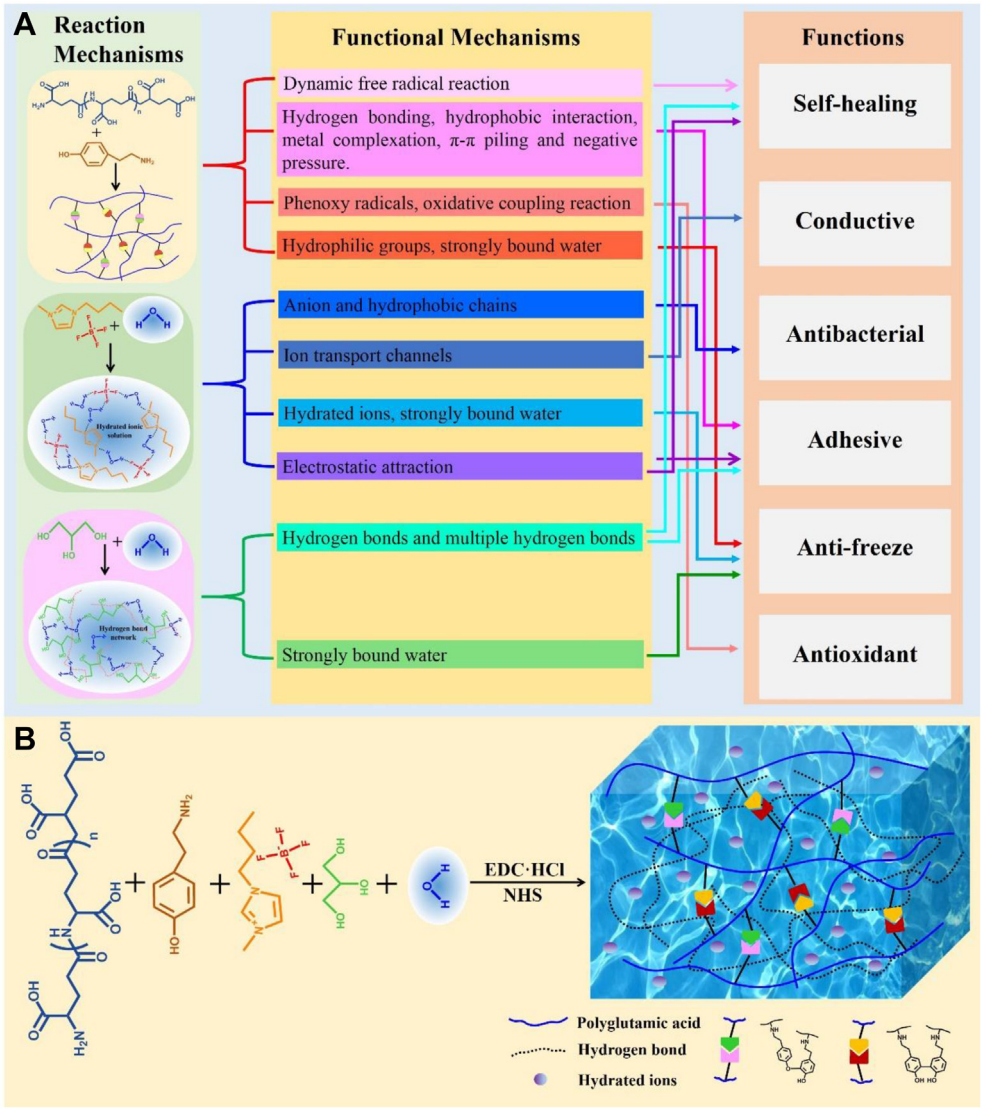

Fig. 1. (A) Strategy and mechanism for the design of an electromechanical dual self-healing multifunctional hydrogel. (B) Preparation of hydrogel.

Co., Ltd. (Chengdu, China) and Henan Lihua Pharmaceutical Co., Ltd. (Anyang, China), respectively. All the previously mentioned materials were used without further purification. Ultrapure water was used throughout the experiment.

2.2. Preparation of hydrogels

The weight (gram) of ultrapure water, [BMIM][BF_4] and glycerol were listed in Table S1. First, different weights of ultrapure water, [BMIM] [BF_4], and glycerol were mixed to form a mixed solution, then 1.4 g of PGA, and 0.6 g of Tyr·HCl were dissolved in the previously mixed solution and stirred at room temperature (25°C) until it dissolved completely to form a homogeneous solution, then 0.6 g of EDC, and 0.6 g of NHS were mixed with the solution under vigorous stirring. After few minutes, a hydrogel was formed at room temperature. The contrast sample polyglutamic acid-lysine (PGA-Ly) hydrogel was prepared according to reference [19]. Briefly, 1.4 g of PGA and 0.6 g of Ly were dissolved in 10 mL of distilled water under room temperature to form a solution and then 0.8 g of EDC and 0.4 g of NHS were mixed with the solution under vigorous stirring. After few minutes, the PGA-Ly hydrogel was formed at room temperature.

2.3. FT-IR characterization

The analysis of the material composition was performed using an FT-IR spectrometer (Spectrum One, Perkin Elmer, Norwalk, USA). Two milligrams of each tested sample was carefully mixed with 200 mg of KBr (infrared grade), ground and then pressed into discs for the measurements. The spectra were recorded from 400 to 4000 per cm wavenumber at a 4 per cm resolution, averaging 64 scans.

2.4. Swelling characterization of hydrogels

The as-prepared hydrogels were immersed in phosphate-buffered saline (PBS) until a swelling equilibrium was attained. The swelling ratio of the gels was calculated from the following equation:

$$SR = (Ws - Wd) / Wd*100\%$$

where W_s is the mass of swollen hydrogel and W_d is the mass of dried hydrogel.

2.5. Degradation characterization of hydrogels

The degradation of the hydrogels was performed in a conical flask filled with 10 mL of PBS (pH = 7.4). The degradation experiments were conducted by incubating the hydrogels in a thermostatic bath at 37°C and by determining the weight loss after recovery of the samples at predetermined time intervals. At the investigated time points, the samples were removed from the PBS medium and then lyophilized. The degradation was assessed by measuring the weight ratio (%), which was defined with the following expression:

$$\text{Weight ratio}(\%) = W_t/W_0* \ 100\%$$

here, W_0 and Wt are the weight of the gels before and after degradation, respectively.

2.6. Rheological measurement

H-30%IL-G3hydrogel was used for testing. Rheological measurement was carried out using a DHR-1 (TA Instruments, USA) rheometer with a parallel plate geometry (25 mm diameter acrylic plate). Shear storage and shear loss moduli (G′ and G″, respectively) were obtained at constant deformation (10%) and temperature (25°C) with increasing frequency (from 0.1 to 100 Hz). G′ and G″ were also obtained at constant deformation (10%), temperature (25°C) and frequency (1 Hz) with increasing time (from 0 s to 1200 s), hydrogel was synthesized and applied to the bottom plate of the rheometer immediately. G′ and G″ were also obtained at temperature (25°C) and frequency (1 Hz) with increasing strain (from 1% to 1000%).

2.7. Mechanical characterization of hydrogels

The compressive stress–strain measurement of the hydrogels was performed using an Instron-5967 universal testing system at a loading velocity of 15 mm/min in air. During testing, the tested samples with cylinder shape (~8 mm in diameter and ~10 mm in initial thickness) were placed on a metal plate. The tensile stress–strain measurement of the hydrogel was conducted on the same universal testing system at a deformation rate of 15 mm/min in air. The test was carried out on dumbbell-shaped samples with the standard JIS-K6251-7 size (25 mm [l] × 2–3 mm (d) × 5 mm (w)). The work of extension at fracture Wb (J/m^2), a parameter that characterizes the work required to fracture the sample per unit volume, was calculated from the area below the tensile stress–strain curve until fracture. For the cyclic tensile test, the samples were stretched at a velocity of 15 mm/min close to a 500% extension ratio at room temperature and then were moved back to the initial displacement after 1 min at the same velocity of stretching. After a minute's rest, the hydrogels were stretched for second tensile test to study their self-recovery behavior. Totally, five cycles were conducted. The cyclic tensile test used H-30%IL-G3hydrogel.

2.8. Electrical conductivity measurement

The top-bottom electrical conductivity of the hydrogels was tested by a four-probe method using a potential state (CHI 660, Chenhua). The schematic illustration of the setup is shown Fig. S1. The conductivity (κ, S/cm) was calculated according to the equation:

$$\kappa = (I / V)(L / A)$$

where V (V) is the measured voltage, I (A) is the current provided by the potential state, A (cm^2) is the cross-section area of the sample, and L (cm) is the distance between the two probes.

Real-time I–t curves were recorded using an electrochemical work station (CHI660E, Chenhua) at a constant voltage of 1 V. The $\Delta R/R_0$ of the deformed hydrogels was calculated as follows:

$$\Delta R = (|R_t - R_0|) / R_0$$

where R_0 and Rt are the resistances of the original ionic skin and the same ionic skin that is stretched or pressed, respectively.

The strain sensitivity of the sensor was calculated by gauge factor (GF), which was the ratio of relative resistance change (ΔR/R0) to the strain (ε). The value of GF was calculated by the following equation:

$$GF = (\Delta R / R_0) / \varepsilon$$

2.9. Self-healing characterization of hydrogels

To investigate the self-healing ability of the samples clearly, the hydrogels were stained in red using edible pigment, which has no influence on self-healing. All the hydrogels were cut into half pieces and then one red half piece and another half piece without dye joined together end to end into a whole one. The self-healing process was investigated at 25°C for 5 min, 1 h, and 2 h, respectively. The self-healing ability of the hydrogels was characterized by using the ratio of the tensile strength of the hydrogels after self-healing to the original tensile strength. The previously mentioned tests all used H-30%IL-G3hydrogel.

2.10. Frostbite test

The frostbite model on Sprague Dawley (SD) rats' back skin was made to demonstrate the biomedical applications of antifreezing hydrogel. The model and experiment procedure were set up based on the method reported by the literature [20,21]. Three female SD rats weighing 180–220 g were used. All rats were divided into three groups: (1) bare group; (2) H hydrogel-treated group; and (3) H-30%IL-G3 hydrogel--treated group. The used hydrogels were listed in Table S1. Before testing, the dorsal skin surface was shaved and cleaned before experiment. The rats were anesthetized by receiving intraperitoneal injection of pentobarbital (2 wt%, 2 mL/kg). The experiments were performed in accordance with protocols approved by the local ethical committee and laboratory animal administration rules of China. A round steel coin with a smooth surface, a diameter of 2.5 cm, and a thickness of 2 mm was immersed in liquid nitrogen tanks for at least 2 h to make it deeply cooled to −196°C. The coin was then taken out and immediately and tightly attached to the skin of the anesthetized rat for 15 s and repeated three times. For the histological studies, the rats were sacrificed by anesthesia. The rats' skin was removed and fixed in 10% formalin buffer. After that, it was embedded in paraffin, the pathological section was prepared, and then the morphological change of the sections stained with hematoxylin and eosin (H&E) was observed under a microscope.

2.11. Antibacterial test

Before the antibacterial experiments with the hydrogels, *S. aureus* and *E. coli* were grown in a Luria-Bertani broth medium (LB) at 37°C for 24 h. The concentration of bacteria used in the experiments was characterized by the optical density at a wavelength of 600 nm (OD_{600}). Here, the OD_{600} nm values of bacteria suspensions were determined to be about 0.1. Colony counting method was used for measuring the antibacterial activities of the hydrogels. Using a typical procedure, the bacteria suspension was dropped onto the surface of the polymeric membrane ($1.5 \times 1.5\ cm^2$) in the plates and incubated at 37°C for 4 h. PBS was used as control. Then 20 μL of the bacteria suspension was dropped onto the culture plate containing agar medium. After being incubated at 37°C for 24 h, the count for viable colonies of bacteria was recorded. Bacterial viabilities after contacting with hydrogels were compared with the number of colonies from PBS control.

2.12. Antioxidant efficiency of hydrogels

The antioxidant efficiency of hydrogels was evaluated by the method of scavenging the stable 1, 1-diphenyl-2-picrylhydrazyl (DPPH)-free radical. The H-30%IL-G3 hydrogel was cut into homogenate using tissue grinder and subsequently dispersed in ethanol at the different concentrations (0.01 mg/mL, 0.05 mg/mL, 0.10 mg/mL, and 0.15 mg/mL) to prepare hydrogel dispersion liquid with different concentrations of hydrogel, respectively. Afterward, 1 mL of DPPH (100 μM ethanol solution) was dispersed in 5 mL of these different hydrogel dispersion liquid. The mixture was stirred and incubated in a dark place for half an hour. Next, the wavelength of DPPH was scanned using a UV–vis spectrophotometer. The degradation of DPPH was calculated by using the following formula:

$$\text{DPPH scavenging } \% = (A_B - A_H) / A_B \times 100$$

where A_B and A_H are the absorption of the blank (DPPH + ethanol) and the hydrogel (DPPH + ethanol + hydrogel) at the wavelength of 517 nm, respectively.

2.13. Detection of reactive oxygen species secreted by cells

Reactive oxygen species (ROS) assay kit (Shanghai Yisheng Biotechnology Co., Ltd.) was used to detect the ROS secreted by cells. L929 cells with exponential growth were collected and then they were made into cell suspension with serum-free medium (the cell concentration was 1×10^6 cells/mL) and divided into two groups (the experimental group used H-30%IL-G3 hydrogel and the control group used PGA-Ly hydrogel prepared by our research group) added different hydrogels and then added DCFH (the final concentration was 10 M) and then incubated 30 min at 37° centigrade. The fluorescence intensity (excitation wavelength = 488 nm and emission wavelength = 525 nm) was detected by flow cytometry. After the cells were incubated with the hydrogel in the 24-hole plate (1×10^4 cells per well) for 24 h, the cell medium was removed, the cells were washed with PBS for three times, then the PBS of 1mL/well was added, the DCFH was added (the final concentration was 10 M), and the 30 min was incubated at 37° centigrade.

2.14. Adhesiveness of hydrogels

The tissue adhesiveness of the hydrogels was characterized by a tensile adhesion test using porcine skin, glass, stainless sheet steel, and Teflon sheet to mimic the natural tissue on a universal mechanical testing machine (Instron 5567). Briefly, porcine skin (glass, nitrile butadiene rubber [NBR], and Teflon sheet, respectively) was used as the represented skin tissue. The hydrogel samples were adhered to the porcine skins (glass, NBR, and Teflon sheet, respectively) with a bonded area of 25 mm × 20 mm. Then the samples were immediately pulled to failure by a universal testing machine with a crosshead speed of 5 mm/min. Lab-shear strength tests were performed with different substrates (glasses, NBR, polytetrafluoroethylene [PTFE], and pigskin). The specimens were prepared according to Zadeh's work by gluing two identical plates (length × width × thickness = $75 \times 20 \times 1\ mm^3$) with a junction contact area of $4\ cm^2$ using 0.2 g hydrogels. The lap joint was compressed under a 300 g weight for 10 min, and then the two ends of the substrates were mechanically clamped to prevent undesired changes of the junction contact area. Subsequently, the adhesion test was immediately conducted at a crosshead speed of 2 mm/min until the occurrence of separation. The adhesion strength was calculated by the maximum load divided by the initial bonded area. Each sample was tested a minimum of three times and averaged [22,23]. The adhesion strength was calculated by the measured maximum strength divided by the bonded area. The above tests all used H-30%IL-G3hydrogel.

2.15. Hemolytic activity assay

The hydrogels were freeze-dried and then immediately grounded into a powder using a mortar and subsequently dispersed in PBS at the different concentrations (5 mg/mL, 10 mg/mL, and 15 mg/mL) to prepare hydrogel dispersion liquids. Rat blood was centrifuged at 2000r/min for 10 min at 4°C, and the erythrocytes were diluted in PBS to obtain a 2% (v/v) erythrocyte suspension after three times of washing using PBS. Erythrocyte suspension of 0.1 mL was mixed with 50 mL of the hydrogel dispersion liquid, PBS, or 0.1% Triton X-100, and the mixture was incubated at 37°C for 1 h. After centrifuging at 4000r/min for 10 min, 200 μL of the supernatants were transferred into a new 96-well plate, and OD_{540} was measured using a microplate reader. PBS and 0.1% (v/v) Triton X-100 served as the negative and positive controls, respectively. The hemolysis percentage of the hydrogels was calculated using the equation: hemolysis (%) = ([As – Ap])/([At − Ap]) × 100%, where As, Ap, and At represent the OD540 of the supernatants from the erythrocyte suspension treated with the hydrogel dispersion, PBS, and 0.1% Triton X-100, respectively.

2.16. Evaluation of biocompatibility

For in vitro cell experiments, all powder materials were irradiated under UV light for 2 h and distilled water was sterilized by autoclaving. The hydrogels were prepared under aseptic conditions. The investigated hydrogels were coated on glass discs using a spinning coater and then

they were immersed in 75% ethanol for 2 h for sterilization and followed by rinsing three times with PBS before cell culture. The biocompatibility of hydrogels was evaluated by fibroblast cells from rats. The blank glass discs and degradation solution (H-30%IL-G3, after degradation for 1 week) were sterilized under high-pressure steam, and then blank glass discs were put in 24-well plates and used as the control groups while those adding 1 mL of degradation solution were used as the degradation groups. And then they were put in 24-well plates for cell culture at 37°C in a 5% CO_2 atmosphere with medium replacement every 2 days. The investigated time points were days 1, 3, 5, and 7. Cell proliferation was determined using an MTT (3-{4, 5-dimethylthiazol-2yl}-2, 5-diphenyl-2H-tetrazolium bromide) assay. After 4 h of adding 20 mL of MTT, excess medium was removed, and dimethyl sulfoxide (DMSO) was added to dissolve the formazan crystal. And then 100 mL of DMSO was added to each well, and the absorbance was measured at 570 nm with an enzyme-linked immunosorbent assay reader. The results were expressed as percentages relative to the data obtained with the blank control. Dual-fluorescence viability, using acridine orange (AO) and propidium iodide (PI), was used for the accurate viability analysis of the primary cells in our study. AO is permeable to both live and dead cells and stains all nucleated cells to generate a green fluorescence, whereas PI enters dead cells with compromised membranes and stains all dead nucleated cells to generate a red fluorescence. As a result, all live nucleated cells were fluorescent green, whereas all dead nucleated cell ones were red. After cell culture for 5 days, the cells were incubated with AO and PI (both 5 mM) at 37 for 10 min. The supernatant medium and excess dye were removed by washing three times with PBS, and then the cells were photographed using an Olympus fluorescence microscope equipped with a digital camera. After cell culture for 5 days, cells were examined by F-actin/4′-6-diamidino-2-phenylindole (DAPI) staining. In brief, cells were rinsed twice with PBS and fixed in 4% paraformaldehyde for 20 min at room temperature and then rinsed three times with the PBS. After that, these cells were incubated with phalloidin for 40 min at 37°C in the dark and then rinsed three times with the PBS. The nuclei were counterstained with 4′-6-diamidino-2-phenylindole for visualization. Microscopy observation was performed using an Olympus fluorescence microscope equipped with a digital camera and Image Proplus. After cell culture for 7 days, the cells were washed with PBS for three times, then 60min was fixed with 4% paraformaldehyde, and then α-SMA immunohistochemical staining was performed with reference to the literature [6]. Microscopy observation of the positive was performed using an Olympus fluorescence microscope equipped with a digital camera and Image Proplus.

2.17. Rat model establishment and wound healing examination

Animal experiments were conducted according to the National Institutes of Health's Guide for the Care and Use of Laboratory Animals. All experimental protocols were approved and performed in accordance with the guidelines of the Animal Ethics Committee of Southwest Jiaotong University. Briefly, adult male rats were anesthetized with 10% pentobarbital. Full-thickness wounds (φ = 1.5 cm) were made on the back of each rat using medical scissors and divided into different groups. Medical gauze and H-30%IL-G3 hydrogel were used as dressing in the control group and the hydrogel group, respectively. For the hydrogel + electrical stimulation (ES) group, the H-30%IL-G3 hydrogel was placed to cover the wound, and ES (AC, 5 V, 40 Hz) was applied through the hydrogel for 1 h per day. Each rat was individually housed in a cage. At 0, 5, 10, and 15 d after the operations, the wound situations were recorded using a digital camera and measured by Image J software (NIH, USA). The residual wound area was calculated by the following formula:

$$\text{Residual wound area}(\%) = S_n/S_0 \times 100\%$$

(S_0: the initial wound area and Sn: the wound area at different time points).

For the histopathologic examination, the regenerated skin was collected and fixed with 10% buffered formalin followed by embedment in paraffin. The sections were stained with H&E and Masson's trichrome reagents and observed under a microscope (Nikon, Japan).

2.18. In vitro scratch assay

Fibroblasts were seeded in a 12-well plate (1×10^6 cells/well) and cultured for 48 h to form a confluent cell monolayer. The cell monolayer was scratched with a sterile 200 mL pipette tip in a straight line to mimic an incisional wound. The experiments were divided into different groups: namely, the control group, the H-30%IL-G3group, and the H-30%IL-G3 + ES group. In the control group, the cells were left untreated, whereas for the H-30%IL-G3 group, the H-30%IL-G3 hydrogel was placed on the top of the cell layer to cover the scratch. For the H-30%IL-G3 + ES group, the H-30%IL-G3 hydrogel was also placed to cover the scratch, and silver wires were inserted in the two ends of the hydrogel to ensure good electrical contact and then connected to the external current resource with alligator clips. The schematic illustration of the setup is shown in Fig. S2. ES was conducted with AC (5 V, 40 Hz) for 1 h, and the healing process was monitored by taking the images of the scratch using a microscope. A marker was made on the bottom of each well to ensure that the same position was photographed each time.

2.19. Gene expression

According to reference [24], after 1 h of ES (AC, 5 V, 40 Hz), the fibroblasts in the different experimental groups as mentioned previously were trypsinized and centrifuged at 2000r/min for 15 min. The total RNA was extracted with RNA extraction solution (Wuhan ServiceBio Technology Co. Ltd, China) according to the manufacturer's instructions. The purity and concentration of the extracted RNA were assessed using a NanoDropTM 2000 spectrophotometer (ThermoFisher, China). The total RNA solution was diluted into a 200 ng/μL of solution with HycloneTM Molecular Biology Grade Water (GE Life Sciences, China), and complementary DNA (cDNA) was synthesized using a RevertAid First Strand cDNA Synthesis Kit (Thermo Scientific, China) following the manufacturer's instructions. Quantitative reverse transcriptase polymerase chain reaction (qRT-PCR) was then conducted with an Applied Biosystems®SteponePlusTMqRT-PCR system (ThermoFisher, China). The sequences of the primers were listed in Supplementary Table S2. The housekeeping gene was b-actin, and the expression levels were calculated using the $2^{-\Delta\Delta Ct}$ method.

2.20. Statistical analysis

SPSS was used to analyze all quantitative data, all of which were expressed as mean ± standard deviation. Each group had at least five samples, and *t*-test was used to evaluate the statistical difference between samples.

3. Results and discussion

3.1. FT-IR characterization

As shown in Fig. S3, the FT-IR spectrum of the PGA-Tyr hydrogel displayed the peaks at 3400 per cm assigned to the combination of O–H and N–H bending vibrations, at 1645 per cm for amide I and at 1567 per cm for amide II, respectively, as well as the peaks at 1710 per cm and 1218 per cm ascribed to the vibrations of the Ph-Ph and C–O–C linkages, respectively [25,26]. From these results, we concluded that C–O–C and/or Ph-Ph coupling occurred between the phenolic hydroxyl groups of the products, and there existed an amide reaction between Tyr and PGA. From the IR spectra of H-30%IL hydrogel, it can be seen that the characteristic peaks H-30%IL are just the superposition of the respective characteristic peaks of both H (PGA-Tyr) hydrogel and IL, and no new

peaks were observed and only the absorption peak at 3400 per cm was widened, indicating that no chemical bond was formed between IL and hydrogel network and that only intermolecular hydrogen bonding interaction was enhanced. Compared with H (PGA-Tyr) hydrogel, the characteristic absorption peak of H-G3 hydrogel shifted to low wavenumber, indicating that a large number of hydrogen bonds were formed in the hydrogel system [27]. The infrared absorption spectra of H-30% IL-G3 hydrogel also showed that all the characteristic absorption peaks shifted to low wavenumber and that the absorption peak at 3400 per cm was broadened, but no new absorption peaks appeared, indicated that no chemical reaction was formed between ILs and glycerol in the hydrogel system.

3.2. Mechanical, electrical, and self-healing properties

We have developed a dual network hydrogel based on reversible chemical cross-linking at room temperature as the first network skeleton and physical cross-linking as the second network. The physical and chemical bonds in the network structure can be reversibly broken and reorganized to dissipate energy effectively, which can endow hydrogels with high rigidity, strength and fatigue resistance, quick recovery, and good self-healing properties [13,28,29]. The zwitterionic ions that are dispersed in the gel skeleton can form a second functional network based on their electrostatic dipole interaction and hydrogen bond self-cross-linking, which not only enhances the mechanical properties of hydrogels but also provides zwitterionic groups as ion transport channels, giving excellent ionic conductivity and strain sensitivity of hydrogels. The rheological results show that the initial storage modulus (G′) was less than the loss modulus (G″), showing a fluid state (Fig. 2A–C). As time went on, both G′ and G″ increased, but G′ increased faster, and then G′ was equal to G″ at a certain time point. When the gel point was reached, the G′ and G″ increased further and finally reached equilibrium; with the passage of time, G′ would be greater than G″, showing that a stable three-dimensional network structure and a solid state were forming in the gel. And then we further studied the viscoelastic properties of hydrogels. At 1% constant strain, the hydrogel had higher storage modulus (G′) and loss modulus (G″), and G′ was greater than G″ in the frequency range of 0.01–100 Hz. With the increase of frequency, the G′ value was up to 1 MPa, indicating that there existed a stable cross-linking network in the hydrogel. If the frequency was kept constant within the strain range of 1%–1000%, the G′ and G″ of hydrogel did not change significantly. The whole gel system was in the linear elastic stage, indicating that the hydrogel had good elasticity. In the cyclic compression test (Fig. 2D, F), the range of compression strain of the hydrogel was set between 0% and 90%. When the load was completely released, each compression cycle curve could well repeat the previous cycle curve, showing good compression cycle stability. In the stress tests (Fig. 2G and H), it can be seen from the stress–strain curve that the elongation at break of the hydrogel was as high as 2600%, and the breaking strength was 1.05 MPa. And then the maximum tensile strain of the hydrogel was set to 500% and cyclic loading tests were carried out. The results showed that hydrogel did not generate large energy dissipation during cyclic stretching process, and its elastic modulus increased with the increase of both loading times and maximum tensile strain. This should be attributed

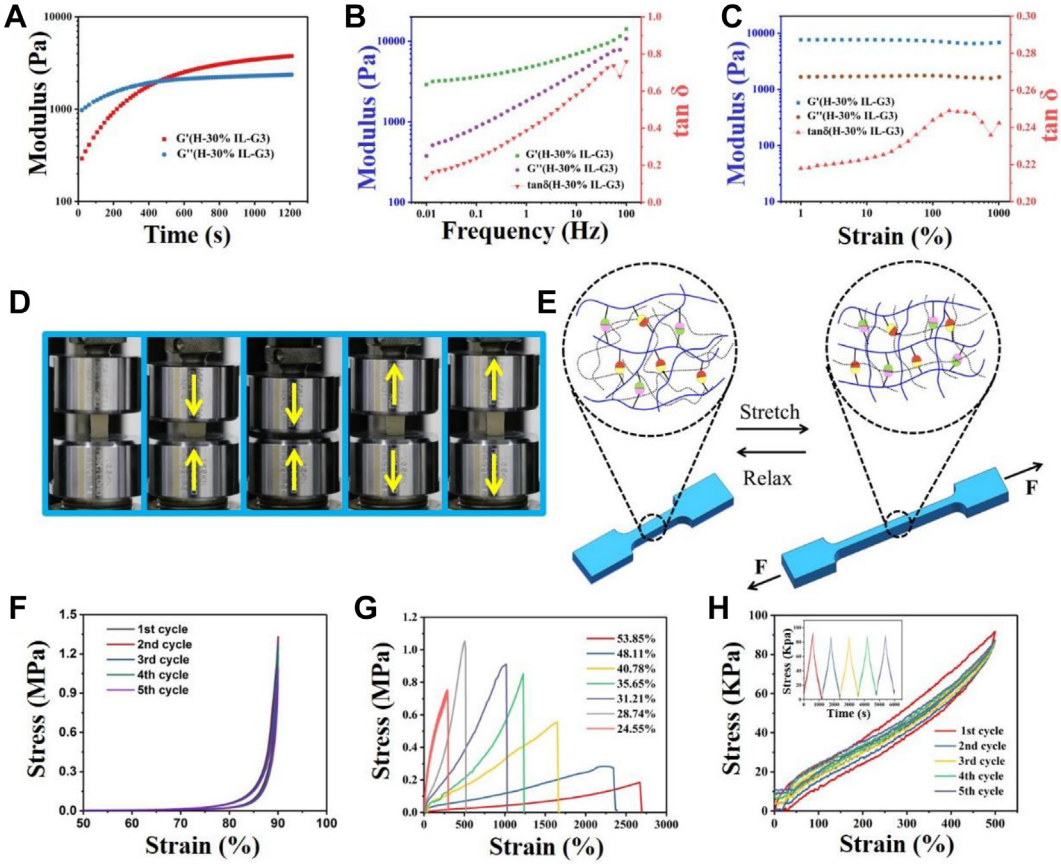

Fig. 2. (A) G′ and G″ curves of hydrogel, tested from 0 to 1200s of time. (B) The G′ and G″ curves of hydrogel, tested in a frequency range of 0.01–100 Hz. (C) G′ and G″ curves of hydrogel, tested in a strain range of 1%–1000%. (D) Images of the as-prepared hydrogel during the loading and unloading process. (E) Schematic diagram of the "force-enhanced" effect during stretching. At the original stage, some groups are wrapped by intertwined polymer chains and do not cross-link; at the tension stage, the groups that are wrapped are re-exposed at stress and then the adjacent groups are further crosslinked. (F) Cyclic compression stress–time curves at 90% strain. (G) Tensile stress–strain curves of hydrogels with different water content. (H) Typical successive loading–unloading tensile tests and stress–time tensile curves of hydrogel for five cycles at 500% strain. Inset graph: stress–time tensile curves.

to the 'force induced enhancement' effect (Fig. 2E) [30]. During the stretching process, the curly polymer chain is stretched by strain, thus exposing more hidden phenolic hydroxyl and carboxyl groups, further cross-linking adjacent groups, increasing the cross-linking point, and improving the elastic modulus. The excellent mechanical properties and rapid recovery properties of hydrogels benefit from the synergistic effect of the hydrogel reversible chemical bonding network and the physical bonding network of multiple hydrogen bonds, π–π stacking, and electrostatic interaction.

Meanwhile, the ionic circuits were achieved by the migration of cations and anions in hydrated ILs [31] to endow the hydrogel with good ionic conductivity [32,33]. Such ionic conductive hydrogel will have higher conductivity than the electron conductive hydrogel, prepared by composing the conductive polymer, because it has higher concentration of counterions as the charge carrier [34]. The effect of IL ratio on the conductivity of the hydrogel was then investigated (Fig. 3A and B). The results showed that the conductivity of the hydrogel increased significantly, which reached 25.4 mS/cm when the IL ratio was 30% with the increase of IL ratio (Fig. 3B). However, after the addition of glycerol, the conductivity of the gel decreased with the increase of glycerol content. This may be attributed to the insulation properties of glycerol itself [35].

Although there have been some reports on the hydrogels that can be conductive and self-healable indeed; however, by our knowledge, there are few reports on the hydrogels that can be conductive and self-healable under stress conditions. To realize real electrical self-healing, it is necessary to investigate the electrical self-healing performance of materials under service conditions, especially under tensile stress. That is to say, only when the complete mechanical self-healing is achieved can the electrical self-healing and the stability of electrical properties under service conditions be guaranteed. Based on this, we propose the idea of constructing a dual network gel through mechanical self-healing network skeleton and electrical self-healing channel to achieve real electrical self-healing. First, the mechanical backbone of the network would be built by dynamic-free radical reaction between tyramine hydrochloride. As the gel network structure is based on dynamic chemical bonding, it has excellent mechanical properties and mechanical self-healing properties. On this basis, we introduced ILs [BMIM][BF_4] with high conductivity, good stability, and antibacterial properties, where ion $[BF_4]^-$ can form hydrogen bonds with water and hydrated ions, thus forming a three-dimensional conductive network structure and then giving the hydrogel good conductivity [15]. The advantage of this structure is that once the damaged mechanical polymer skeleton is repaired, the network structure of its aqueous phase is also restored. When water is combined with IL, the network structure of aqueous phase then becomes hydrated ion network. The conductive hydrogels are often prepared by adding conducting polymers or conducting particles in the hydrogels, and their conductive channels will be damaged and difficult to be rebuilt once they are destroyed by external forces. However, the ionic conductive hydrogels prepared in this work are characterized by the rapid reorganization of hydrogen bonds after breakage. Their conductive channel can be quickly rebuilt after damage, giving excellent conductivity and self-healing property of the hydrogel. Therefore, such hydrogels with hydrated ion network structure can be regarded as a real electrical self-healing material. In addition, as the result of the inherent antibacterial properties of imidazolium cation, it can give good antibacterial properties to hydrogels. Second, our previous studies have found that there are abundant hydroxyl groups on glycerol, thus being able to form dynamic physical bonds with amino and carboxyl groups in the side chain of polymers, which can not only enhance the self-healing properties of the system but also enhance the adhesion properties of the system. Therefore, in this study, dynamic physical bonding and chemical bonding both play a significant role in the mechanical self-healing properties of materials. First, the mechanical self-healing properties of hydrogels were characterized (Fig. 3C–E), from the stress–strain curves of the gel at different healing times (Fig. 3E), it can be seen that the hydrogel that was cut into two pieces can be healed quickly after fitted together, and its mechanical property recovered to 70% of the original just after a few seconds, but after 1 and 2 h, the original tensile strength and elongation at break could reach 90% and 99% of the original sample, respectively. In addition, we also characterized the mechanical self-healing properties of

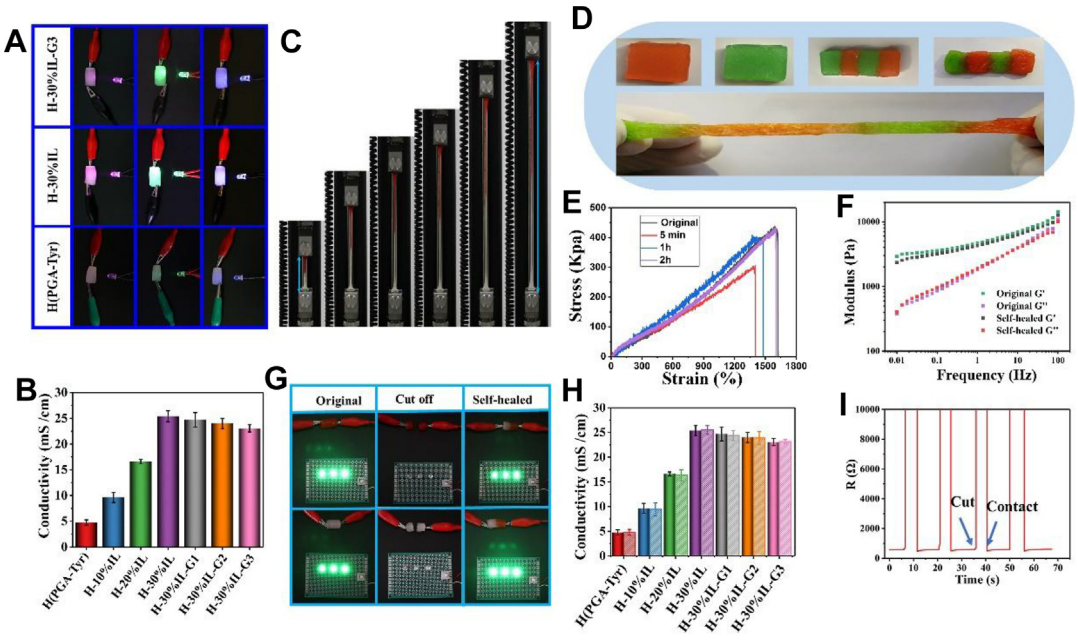

Fig. 3. (A) Illustration of the conductivity properties of the hydrogel for the circuit. (B) Conductivities of various hydrogels. (C) Images of the self-healed hydrogels in tensile strength and elongation during the tensile test. (D) Hydrogel is cut into two pieces and recombined. The fractured hydrogel with an alternative color can be immediately spliced together at room temperature and stretched without failure after 4 h. (E) Stress–strain curves of the original and the self-healed hydrogels at various healing time points at a tensile rate of 15 mm/min. (F) G′ and G″ curves of the original and the 2 h-healed hydrogels, tested in a frequency range of 0.01–100 Hz. (G) Conductive self-healing function behavior of the hydrogel: original hydrogel→ broken hydrogel→ self-healed hydrogel; (H) Conductivities of the original and self-healed hydrogels with different ionic liquid and glycerol contents; (I) Time evolution of the healable process for the conductive hydrogel by the real-time resistance measurements, the R-t curve under several cutting/healing processes.

hydrogels by rheological tests. The results showed that the G′ and G″ of hydrogels were the same as those of the original hydrogel after 2 h of self-healing (G'>G″), and no significant difference was observed for them (Fig. 3F), hence indicating that the hydrogel achieved complete self-healing in mechanical properties.

In the study of electrical properties of electrical self-healing of hydrogels (Fig. 3G–I), it can be observed that the conductive path changed from conduction state to open circuit state when the as-obtained hydrogel was completely cutoff. However, once the broken hydrogel was rejoined together, its electrical properties instantly recovered. Furthermore, we designed a circuit composed of hydrogel and three LED indicator lamps to demonstrate the electrical self-healing performance intuitively. When the hydrogel was cutoff, the LED lamps would switch off. Once the two broken parts were recontacted, the LED lamps would turn on again instantly (Fig. 3G). However, if there is no guarantee of mechanical self-healing, the electrical self-healing performance is just a flash in the pan, and the external tensile stress will make it break quickly and lose the conductive property instantly. Only when the complete mechanical self-healing is realized can the stability of electrical self-healing be ensured. Therefore, we further examined the electrical self-healing properties of hydrogels under service conditions. The relative resistance changes of hydrogels before and after self-healing were investigated under different external stresses. The results showed that the electrical properties of the hydrogels after healing for 2 h were similar to those of the original hydrogels, regardless of tensile stress, bending stress, or compressive stress. Under tensile stress, when the strain was 200%, the conductivity of the hydrogel after healing was 99% of the original hydrogel. When the strain reached 400%, the conductivity of the hydrogel remained at 95% of the original hydrogel. However, the conductivity of the hydrogel after healing was not different from that of the original hydrogel under different compressive stress. Under bending stress, when the curvature was 90°, the conductivity of the hydrogel after healing remained 98% of the original hydrogel. Furthermore, we examined the conductive self-healing properties of the self-healing hydrogels under a variety of complex strains in daily life, such as wrist bending, arm bending, neck bending, knee bending, and laryngeal movement during speaking different words. The results showed that the conductivity of the self-healing hydrogel was basically consistent with that of the original hydrogel.

From the self-healing results, we speculate that physical bonding and chemical bonding play a key role in self-healing at different stages. Physical bonds play a major role at the early stage of self-healing, prompting their rapid self-healing. The introduction of glycerol provides a large number of hydroxyl groups in the hydrogel system, thus causing a large number of hydrogen bonds in the hydrogel. Hydrogen bonds can recombine very rapidly after breaking, which provides the initial traction for self-healing. Moreover, a large number of cations and anions are also introduced into the hydrogel system with the addition of ILs, which not only improves the conductivity of hydrogels but also plays an important role in the process of self-healing because of the electrostatic interaction between cation and anion. Therefore, electrostatic interaction further provides the driving force for self-healing of hydrogels, which makes the broken gel network more firmly integrated and provides a guarantee for subsequent chemical bonding. Reversible chemistry plays an important role in the healing process at the later stage so that the damaged gel network can be rebuilt together to restore the gel network to achieve the entire self-healing of mechanical properties, thus ensuring the permanence of electrical self-healing. In short, the synergistic effect between physical bond and reversible chemical bond enables the gel to self-heal quickly after damage and endows it with excellent self-healing properties and electrical self-healing stability.

3.3. Service performance under extremely cold conditions

The high water content of hydrogel endows it with good flexibility [36], thus presenting excellent performance in the fields of soft electronic devices, soft robots, soft sensors, and soft energy storage devices, as well as in biomedical fields such as wound dressings. However, high water content makes it inevitable to freeze at low temperature, which makes it lose a series of functions, such as conductivity, flexibility, and sensitivity, and its service performance so that its applications will be greatly restricted. Therefore, it is of significance to study the antifreezing properties of hydrogels. Because the crystallization of water molecules is formed through hydrogen bonds, the basic strategy to solve the problem of freezing is to inhibit the formation of hydrogen bonds. Basically, there are three different forms of water molecules in the hydrogel [18]: free water, which can move freely; 'weakly bound water', which has weak interaction with the polymer network; and 'strongly bound water', which has strong interaction with the polymer network. The water molecules of these three different states have completely different freezing temperatures, of which the 'free water' is the most easily frozen, whereas the 'strongly bound water' has very low freezing point, which provides a theoretical guidance for the preparation of low-temperature hydrogel. Obviously, the fundamental way to solve the problem of freezing is to inhibit the formation of hydrogen bond of free water. At present, soluble salts, alcohols, or ILs can be added to the solvent to reduce its freezing point; and functional monomers can also be designed to introduce more groups with strong interaction with water, so as to adjust the interaction between water and polymer network to reduce the proportion of 'free water' to improve antifreezing property. Although there have been some reports of antifreezing hydrogels, for example, some inorganic salts (such as NaCl, $CaCl_2$, and LiCl) have been introduced into hydrogels to improve their antifreezing property [16,37,38]. Vlassak et al. synthesized a series of polyacrylamide sodium alginate double network hydrogel and immersed it in different $CaCl_2$ solutions [16]. When the anion and cation diffused into the hydrogel, the hydrogel was endowed with antifreezing property [16]. However, the introduction of inorganic salt reduced the moisture retention of the hydrogel and affected the stability of the hydrogel. Chen et al. modified polyacrylic acid and prepared an alkaline polyacrylic acid hydrogel [39]. Because of abundant carboxyl group on the polymer chain, the freezing point of the hydrogel dropped to −25°C [39]. Although the modified polymer network could also achieve a certain degree of antifreezing ability, this method is complicated in design and cumbersome in technology.

Based on this, we constructed antifreezing hydrogel use of three mechanisms. On the basis of previous researches, antifreeze hydrogels are constructed through three strategies. First, we designed a hydrogel network by introducing hydrophilic polyglutamic acid and tyramine hydrochloride. In this system, a large number of hydrophilic groups, such as carboxyl group, amino group, and phenolic hydroxyl group, can form a large number of hydrogen bonds with water molecules so that more strongly bound water can form, thus reducing the content of free water and making the material itself have good intrinsic antifreezing properties. Second, after the [BMIM][BF_4] IL with good water solubility and biocompatibility was compounded with water molecules, not only the hydrogen bond interaction between BF_4^- and water molecules (the reported binding energy of BF_4^--H_2O is 45.12 kJ/mol) [15,36] played a dominant role in all hydrogen bond but also could the three hydrogen protons on the imidazole ring form stable hydrogen bond interaction with water molecules (the reported binding energies for them are 33.87 kJ/mol, 34.81 kJ/mol, and 35.71 kJ/mol, respectively, these binding energies are much stronger than the binding energy of 18.8 kJ/mol between water molecules) [18]. With the aid of such stronger hydrogen bond interaction in the system, some of the 'free water' can be converted to hydrated ions with higher binding energy [16], which can reduce the freezing point and endow the hydrogel with good antifreezing properties. Third, we introduced glycerol into the hydrogel system to further reduce the liquid–solid transition temperature of hydrogels [37], thus giving the hydrogel more excellent antifreezing properties. There are three reasons for that. First, the chemical potential of the aqueous solution will decrease compared with that of pure water because of the addition of glycerol, which is an entropic effect and may

be understood by the fact that glycerol contributes to the entropy (S) of the system by enhanced molecular randomness (or number of microstates). Thereby, the aqueous solution of glycerol is in more stable state than the aggregation state of water molecules. Second, hydrogen bonding between hydroxyl groups and water molecules reduces the interactions between water molecules (hydrogen bonds), whereas hydrogen bonding between water and glycerol increases the nucleation barrier for ice crystallization, thus reducing the number of 'free water' molecules and preventing the formation of ice crystals [38–43]. Third, the aggregation of the hydrophobic residues of the glycerol will disturb the three-dimensional H-bond network [44], thus restraining the formation of ice crystals.

It can be detected that the LED indicator could still be lit up even at −60°C (Fig. 4A). This indicates that the carrier channel in the hydrogel is still conductive under extremely low temperature. For the hydrogel with both glycerol and IL, further tests showed that at 25 °C, the brightness of LED was the strongest. The quantitative test results of electrochemical workstation showed that the conductivity reached 23 mS/cm (Fig. 4B). When the temperature decreased from 25°C to −20°C, the conductivity reduced from 23 mS/cm to 18.7 mS/cm, which is due to reduction of charge carriers at low temperature in the hydrogel network [45]. When the temperature further reduced to −40°C, the conductivity was only 9.1 mS/cm. The low temperature differential scanning calorimetry (DSC) curve showed that the hydrogels without glycerol and ILs have free water freezing peaks at −25°C, indicating that the hydrogel itself also has certain antifreezing ability (Fig. 4C). This is because the hydrogel network contains a large number of carboxyl groups, amino groups, and phenolic hydroxyl groups that can form hydrogen bonds with the water molecules, thereby reducing the interaction between the water molecules (hydrogen bonds) and, to a certain extent, preventing the formation of ice crystals. While the freezing peak of free water shifted to −32°C for H-30%IL hydrogel with IL, which should be attributed to the formation of hydrogen bonds between the anion and cation of the IL and the water molecules, thus making some of the free water in the hydrogel changed into a strongly bound water. The freezing temperature further decreased to −40°C for the glycerol-containing H-G3 hydrogel because of the formation of multiple hydrogen bonds between glycerol and free water in the hydrogel. More free water is transformed into strongly bound water and then the freezing temperature of free water reduces. It can be interesting to see that the freezing peak appeared at −54°C, whereas both glycerol and IL were added into the hydrogel, which is much lower than that of the hydrogel with only glycerol or IL. In general, because of the introduction of a large number of hydrogen bonds via the addition of glycerol and ILs, the excellent antifreezing properties of hydrogels have been achieved so that the hydrogel could still maintain a certain electrical conductivity under extremely cold conditions, which can meet the service requirements under extremely cold conditions [46].

To verify the protective effect of the antifreeze hydrogel on the skin at low temperature, frostbite test was carried out on the back skin of rats (Fig. 4D) [47]. The results (Fig. 4E) showed that the group without hydrogel had significant loss of collagen fibers, and the PGA-Tyr hydrogel group also showed some signs of frostbite, whereas the hydrogel group containing IL and glycerol had intact epidermis and collagen fibers.

The previously mentioned results confirm that in extremely low-temperature environment, H-30%IL-G3 hydrogel, used as a sensor or skin dressing, can maintain the stability of both structure and function of the hydrogel well.

3.4. Antibacterial property

The antibacterial properties of hydrogels were tested using a plate counting method and characterized the antibacterial activity of hydrogel to *Escherichia coli* and *Staphylococcus aureus*. As shown in Fig. 5, all the hydrogels had antibacterial activity in different levels, which might be attributed to the antibacterial property of IL itself, and the antibacterial mechanism is as follows: First, through the interaction of anions and anions, the positively charged ILs and negatively charged bacterial cell walls attract each other, and then through some fat-soluble carbon chain structure, the integrity of the bacteria will be destroyed, and eventually, the bacteria will die. The antibacterial capacity of hydrogel increased with the increase of IL content from 10% to 30%. This is because, on the one hand, the content of imidazole ring increases with the increase of the IL content. The positive imidazole ring can destroy the bacterial cell membrane through electrostatic action and negative phosphoric acid group on the bacterial cell membrane [14]; on the other hand, with the increase of the IL content, the content of the hydrophobic chain segment also increases. When contacting with bacteria, more hydrophobic chains can be inserted into the phospholipid bilayer of cell membrane, thus disturbing the cell membrane and leading to the leakage of the cytoplasm

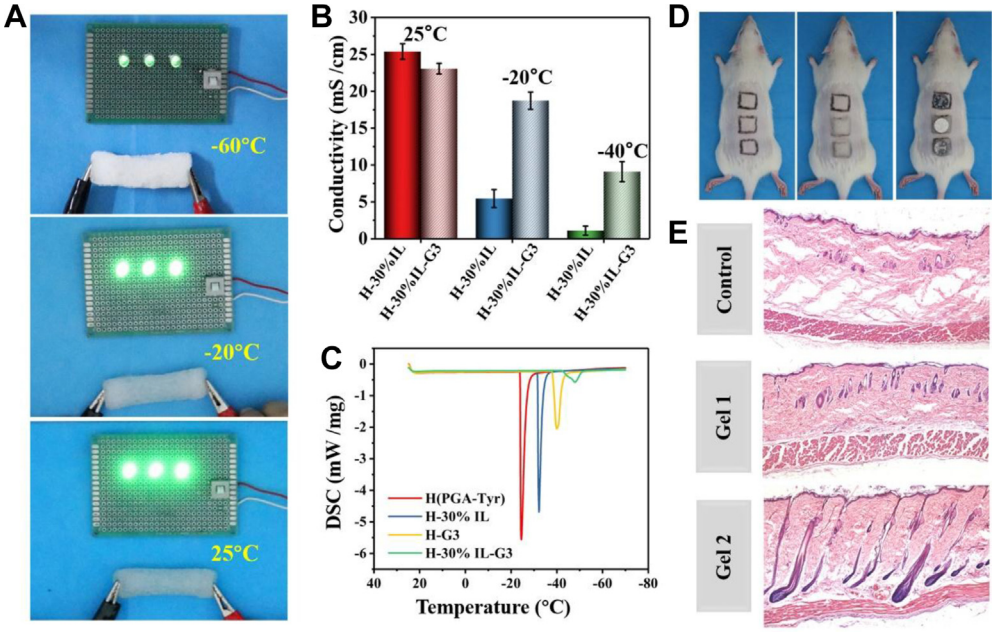

Fig. 4. (A) Circuits comprising hydrogel in series with an LED indicator at different temperature, respectively. (B) Conductivities of H-30%IL and H-30%IL-G3 hydrogels at different temperature, respectively. (C) DSC curves of different hydrogels during cooling. (D) Frostbite model on rats' back skin to demonstrate antifreezing performance of adhesive hydrogel, the process of experiment was presented from the left to the right. Left: the photo of a rat depilated and marked on the back. Middle: photos of the rat after gel 1 (PGA-Tyr) and gel 2 (H30%IL-G3) were attached to the labeled skin area. Right: photos of the rat after the −196°C cold coins were attached to the bare skin and the skin protected by gel 1 and gel 2. (E) Histological microscopy images of the hydrogel-treated skin and the bare skin after frostbite (H&E staining). The composition of the hydrogels (PGA-Tyr and H-30%IL-G3) used for animal experimental is shown in Table S1 (Supporting Information).

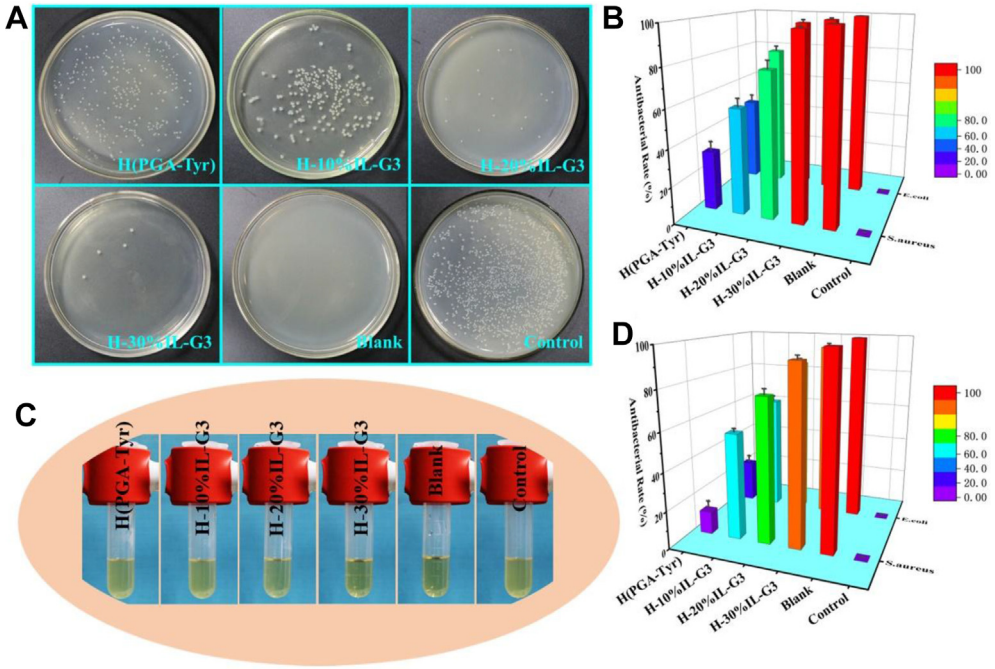

Fig. 5. (A) Images of co-culture of *E. coli* with different hydrogels. (B) Antibacterial rate after co-culture of *E. coli* with different hydrogels using the counting method. (C) Images of co-culture of *S. aureus* with different hydrogel extract solutions, respectively. (D) Antibacterial rate after co-culture of *S. aureus* with different hydrogel extract solutions using the microplate method.

and eventually the bacterial apoptosis [14]. It can be seen from Fig. 5 that the antibacterial activity of hydrogel to *E. coli* is better than that of *S. aureus*, and this may be because of the different cell membrane structure of *E. coli* and *S. aureus*. The negative and hydrophilic properties of the cell membrane of Gram-negative bacteria are higher than those of Gram-positive bacteria. Therefore, we speculate that the positive imidazole ring has stronger electrostatic interaction with Gram-negative bacteria and is more likely to cause bacterial cell death [14,48,49]. This kind of good antibacterial ability of the hydrogel can promote wound healing by reducing the number of pathogenic bacteria and inflammatory reaction [50–52].

3.5. Antioxidant performance

DPPH radical scavenging method was used to evaluate the antioxidant properties of hydrogel [53]. The results showed that the

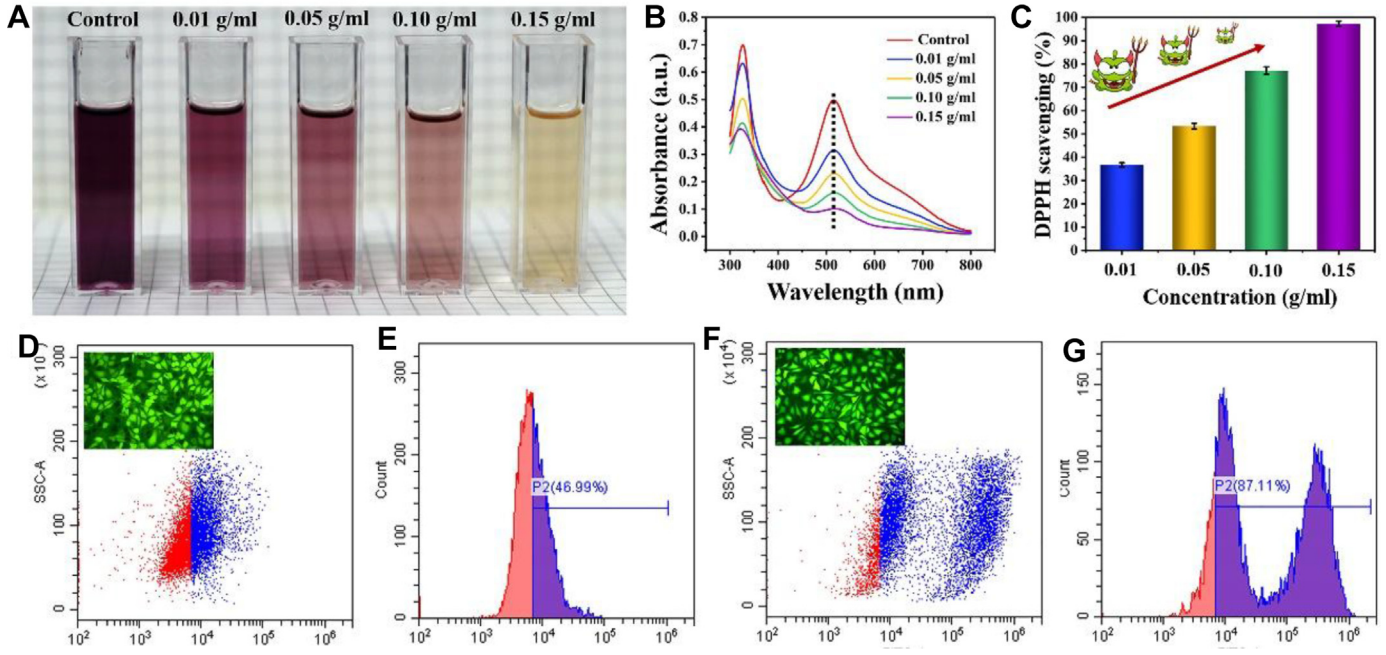

Fig. 6. (A) Photos of DPPH solution coincubated with different weight hydrogels after 0.5 h. (B) UV–vis spectra of DPPH scavenging. (C) DPPH scavenging rate of different concentrations of H-30%IL-G3 hydrogels. (D, E) Quantitative detection for reactive oxygen species (ROS) of cells co-cultured with H-30%IL-G3 hydrogel using flow cytometry, inset: fluorescence images of cells co-cultured with H-30%IL-G3 hydrogel stained using ROS assay kit. (F, G) Quantitative detection for ROS of cells co-cultured with PGA-Ly hydrogel using flow cytometry, inset: fluorescence images of cells co-cultured with PGA-Ly hydrogel stained using ROS assay kit.

dark-colored DPPH radicals became light-colored DPPH-H by reacting with antioxidants, which was detected as a decrease in the absorbance at 517 nm. A gradually improved DPPH radical scavenging activity with the increase in the amount of hydrogel was shown in Fig. 6, indicating that the scavenging efficiency of DPPH radicals increased. When the amount of hydrogel was 0.15 g/mL, the scavenging rate of DPPH radicals reached 97%. The scavenging ability of hydrogels to free radicals might be attributed to the ability of phenolic hydroxyl group to capture free radicals in liquid medium. When they are trapped to form phenoxy radicals [54,55], further oxidative coupling reaction occurs and then the free radicals are consumed. Therefore, the phenolic hydroxyl in hydrogels endows the hydrogel with good antioxidant properties. A large number of research reports indicated that hydrogels with antioxidant properties can reduce the oxidative stress reaction of wounds by eliminating excessive ROS [56–58], thereby preventing cell damage and enhancing cell viability [56,59], which plays a vital role in various stages of wound healing, and has been proved to accelerate wound repair [60].

Based on the fact that the experimental model for detecting ROS is difficult to be implemented in vivo, therefore, an investigation was conducted on the effect of hydrogel on the secretion of ROS by co-culture with cells in vitro to explore the effect of antioxidants on the secretion of ROS. The H-IL30%-G3 hydrogel was used as the experimental group, and the PGA-Lysine hydrogel (PGA-Ly, without free radical cross-linking, supporting information) was used as the control group. The effect of hydrogel on the secretion of ROS was detected using the method previously reported [61]. The results showed that the positive rate of ROS in the control group was much higher than that in the experimental group after 1 h incubation, showing the H-IL30%-G3 hydrogel could repress the production of ROS greatly, which would be beneficial for wound healing.

3.6. Adhesive property

Adhesive property of hydrogels can guarantee broad applications ranging from medical electrodes and human portable devices to tissue repair and wound dressings. The results showed that the as-synthesized hydrogels not only adhere firmly to various organic and inorganic surfaces, including PTFE, glass, plastic, rubber, and steel (Fig. 7A), but also have good adhesion to various biological tissues, including heart, spleen, lung, liver, and skin (Fig. 7B). To quantitatively evaluate adhesive strength, shear measurement was carried out using a universal test machine (Fig. 7C). The quantitative results also showed that the obtained hydrogels have very high adhesion to different substrate (Fig. 7D–G). Especially for NBR, the highest tensile adhesion strength was 1095 KPa, and the highest shear adhesion strength was 503 KPa. Although the adhesion strength of some reported hydrogel materials and metals has reached tens of MPa, their adhesion strength with pigskin was low. For example, Li et al. reported a mineral enhanced polyacrylic acid hydrogel (mineral enhanced polyacrylic acid hydrogel) [62], although its adhesion strength with aluminum substrate could reach 7.71 MPa, its adhesion strength with pig skin was only 50 KPa. Wang et al [63] reported a nanocomposite hydrogel, and its adhesion strength with copper substrate reached 60.5 MPa. However, its adhesion strength with pig skin was only 130.70 KPa. In our study, the tensile and shear adhesive strengths of our hydrogel to pigskin reached 800 KPa and 400 KPa, respectively, which were almost an order of magnitude larger than those biomedical hydrogels previously reported [64,65], showing a good application prospect in biomedical field. This may be because of the following reasons: (1) the introduction of glycerol provides a large number of hydroxyl groups for the system, which can form hydrogen bonds and multiple hydrogen bonds with many substrates [66], and thus greatly improve adhesion; (2) the introduction of [BMIM][BF_4] IL provides a large amount of anion and cation for the hydrogel system, which can cause electrostatic attraction with the substrate to improve adhesion performance; (3) the ortho substituted phenolic groups on tyramine hydrochloride have similar structure to the catechol group of dopamine dopamine (DA) and have high binding affinity to various nucleophiles (such as amine, mercaptan, and imidazole), which can form a bridge between the interface of materials and substrate [65,67,68]; (4) the residual carboxyl groups, amino groups, and phenolic hydroxyl groups in the polymer molecular chain can be reversibly adhered to various solid substrates and biological tissues by hydrogen bonding, hydrophobic interaction, metal complexation, and pion piling on the interface

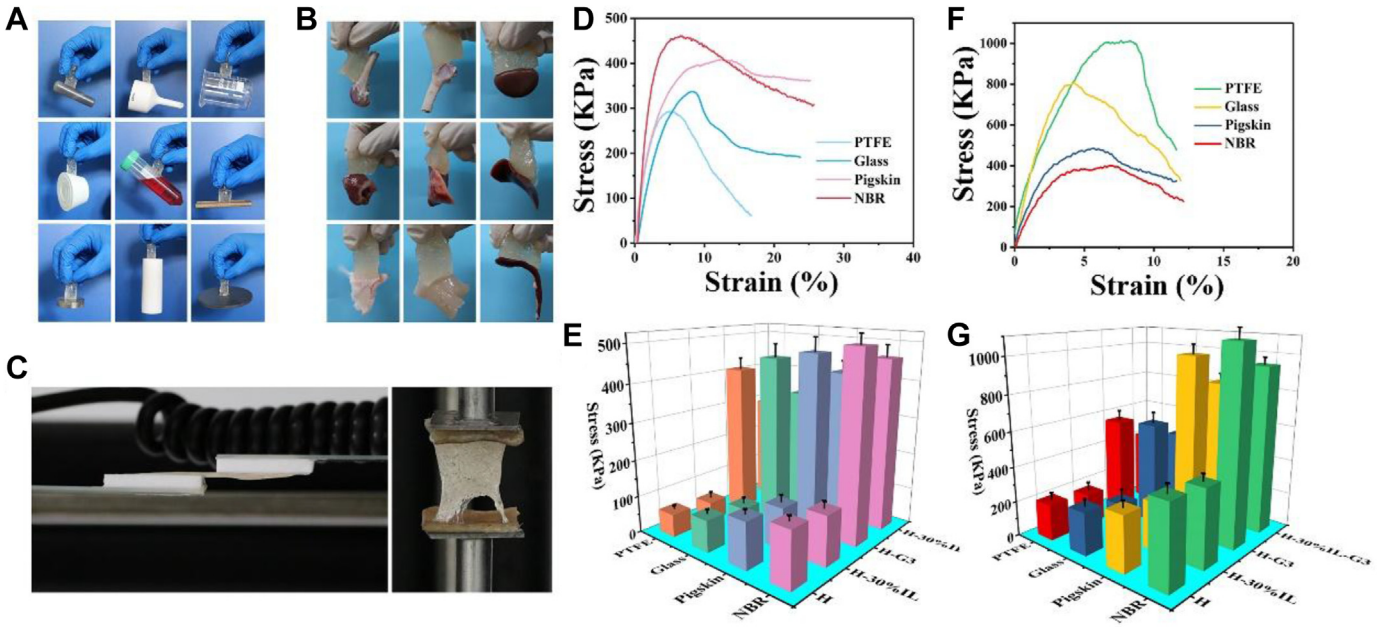

Fig. 7. (A) Adhesive exhibition of hydrogel adhering to diverse materials, including carnelian, ceramics, glass, silica rubber, plastics, wood, stainless steel, PTFE, and graphite. (B) Exhibition of hydrogel adhering to biological tissues, including bone, cartilage, kidney, heart, lung, liver, skin, muscle, and spleen. (C) Images of tensile adhesion test and lap-shear adhesion test. (D) Force-extension curves of lap-shear adhesion test geometry of hydrogels on different substrates. (E) Shear adhesive strength between hydrogels and different substrates. (F) Force-extension curves of tensile adhesion test geometry of hydrogels on different substrates. (G) Tensile adhesive strength between hydrogels and different substrates.

between the material and the substrate [69]; and (5) the hydrogel flexible network has a certain flow property through the physical intersections of polymer chain segments. The slippage or the deformation of the whole network makes it well attached to the surface of the substrate, eliminating air and producing negative pressure. Using such pressure difference can generate enough 'suction', which provides favorable conditions for bonding on the interfaces [30]. The synergistic effect of various factors gives the hydrogel super high adhesion performance. In general, it can be seen from these results that the adhesion properties of hydrogels are closely related to the formation of dynamic physical bonds. Therefore, we suggest that the self-healing performance design concept of dynamic physical bonds can be used to guide the design of adhesion properties. Moreover, the adhesive ability on various major organs should be attributed to the free-catechol groups, which have excellent interfacial binding affinity for nucleophiles (i.e. -NH_2 and -SH groups) often present on the surface of biological tissues.

3.7. Swelling and degradation properties

Swelling ratio was investigated for the as-synthesized hydrogels, which displayed extraordinary swelling properties (Fig. 8A–C). The swelling ratio could reach 2650% in PBS. This is because that PGA and Tyr contained rich hydrophilic groups, such as carboxyl and amino groups, which contributed to great hydration capacity, and thus led to high water-containing content for the PGA-Tyr hydrogels. The high swelling ratio of hydrogels will be beneficial for absorbing the exudates from the wound, thus creating a microenvironment beneficial for the repair of the wound. On the other hand, the as-obtained hydrogels contained a large number of pores so that they could have a large room to hold a large number of water molecules before the swelling equilibrium was achieved. In addition, we also found that adding IL and glycerol could reduce the swelling ratio of hydrogels; this is because of that IL and glycerol can be connected with hydrogel network via hydrogen bonding, which limits the stretching of hydrogel network, thus suppressing the swelling of the hydrogels.

As shown in Fig. 8D, the degradation curve of the hydrogel showed that after 21 days of degradation in PBS solution, the residual mass of the hydrogel was about 20% of the original weight, showing a good degradation property in vitro. Normally, the scab of skin wound can fall off within 5–10 days, which is shorter than the degradation time of the as-obtained hydrogel in vitro when hydrogel is used for skin dressing. Therefore, the as-obtained hydrogel will be suitable for skin dressing. When the as-obtained hydrogel is used in non-aqueous environment (e.g. the atmospheric environment), it is stable and has no degradation and thus can be used for skin sensors.

3.8. Hydrogel for the wound dressing

During skin wound repair, ES therapy as a clinical treatment method has been used for wound healing for more than 50 years, and great progress has been made [52,70,71]. ES can promote cell adhesion, proliferation and differentiation at the material tissue interface, thus enhancing the growth of tissue [72,73]. The activity of fibroblasts and keratinocytes can be improved with the help of conductive dressings supplemented by ES, which plays an important role in the skin healing process [74].

To achieve biomedical applications of conductive self-healing hydrogels, their hemocompatibility and biocompatibility were characterized. The hemocompatibility of the H-30%IL-G3 hydrogel was evaluated by the in vitro hemolysis assay using PBS and Triton X-100 as the negative and positive controls, respectively. The supernatant of the Triton X-100 group shows a bright red color because of significant hemolysis and release of hemoglobin. In contrast, similar to the PBS (a solution that does not induce hemolysis of erythrocytes) group, the supernatants of the hydrogel groups are light yellow colored (Fig. 9A). When the hemolysis rate of the positive group was 100%, even if the weight ratio of the hydrogel increased to 15 mg/mL, the hemolytic rate of all the hydrogel groups was still less than 4% (Fig. 9B). These results indicate the excellent hemocompatibility of the H-30%IL-G3 hydrogel. The biocompatibility of the H-30%IL-G3 hydrogel was evaluated via the

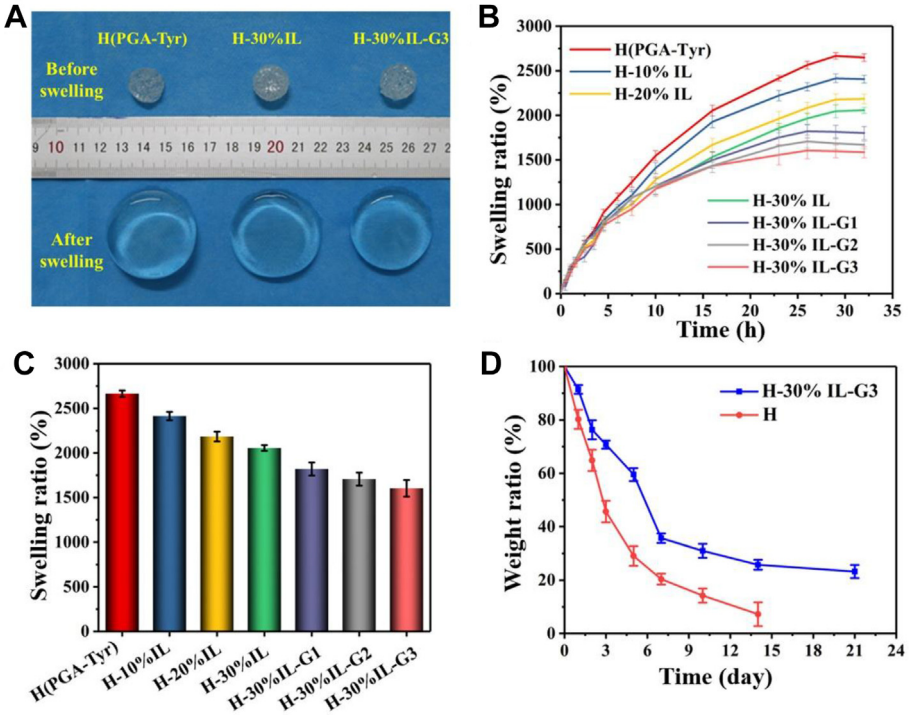

Fig. 8. (A) Images of the hydrogels before and after swelling equilibrium. (B) The swelling curves of hydrogels in PBS buffer solution. (C) The swelling ratios of hydrogels in PBS buffer solution. (D) The weight loss curves of hydrogels.

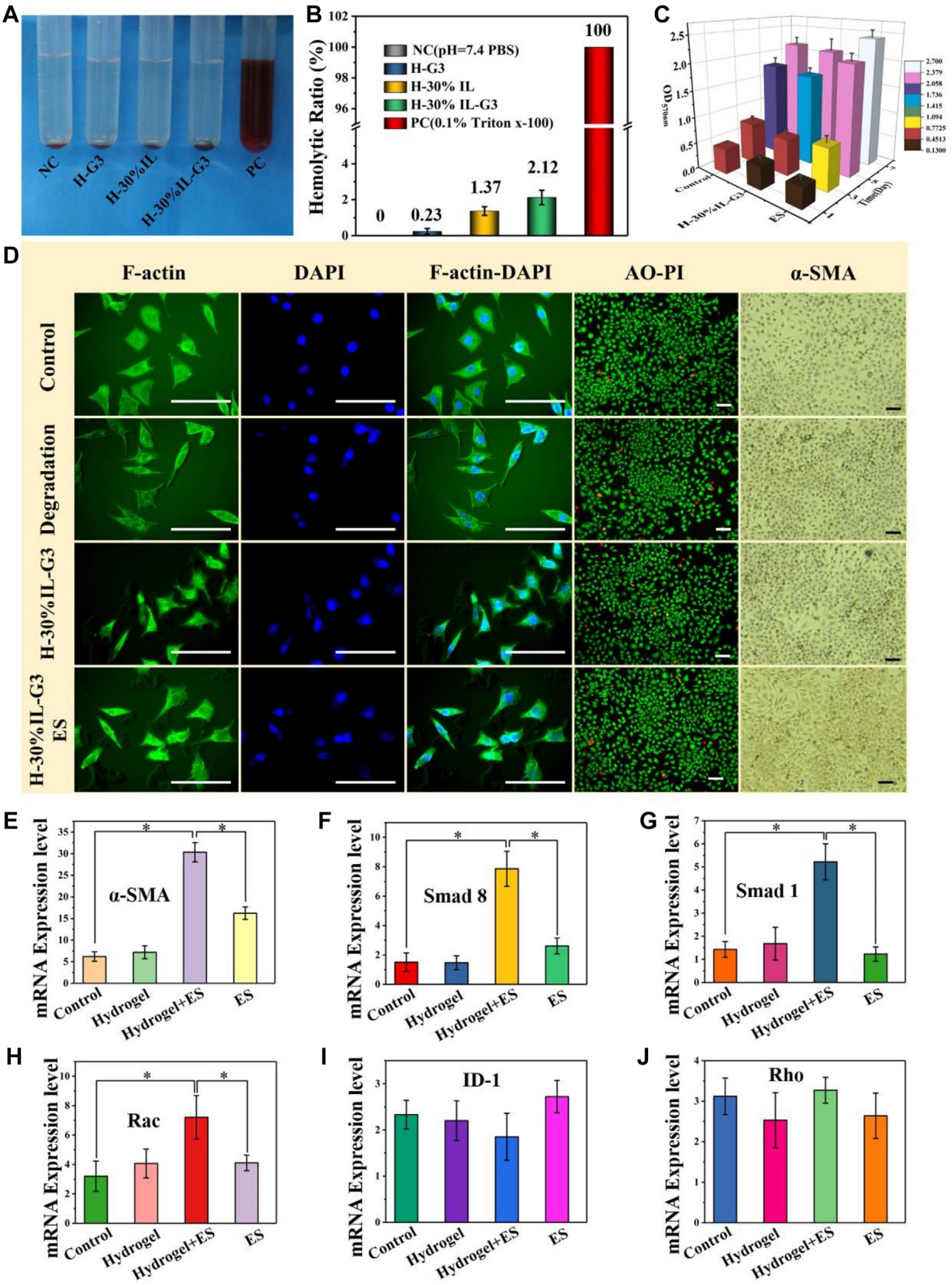

(caption on next page)

co-culture of hydrogels and cells, and MTT results were almost the same for the hydrogel group (Fig. 9C), the degradation product group, and the blank control group. The number of cells increased exponentially with time. In addition, the fluorescent images for the staining of the live/dead cells showed that there were only very few dead cells in all the experimental groups and the cells were distributed evenly and the density was high in all the experimental groups (Fig. 9D). There was no significant difference between any two groups of the hydrogel, degradation liquid, and blank groups. The F-actin/DAPI staining results also showed that the morphology, structure, and density of cells in the hydrogel group and the degradation product group were not significantly different from those in the blank group, and all the cells were in good condition, and the cell structure was intact (Fig. 9D), which shows that hydrogel has no negative effect on cells, demonstrating that the obtained hydrogel has good biocompatibility. At the same time, we investigated the effect of ES (ES) on human skin fibroblasts. MTT, live/death staining, and F-actin/DAPI staining results showed that there was no significant difference between the fibroblasts exposed to ES and those not exposed to ES, which clearly indicated that ES had no toxic effect on human skin fibroblasts.

To study the effect of ES on the migration of fibroblasts, the effect of ES on the migration of fibroblasts by the scratch closure experiment was investigated for the first time. The results showed that the closure speed of the ES group was much faster than that of the group without ES (Fig. S4), which was consistent with the results reported in literature [75], indicating that ES could promote and dominate the migration of fibroblasts. We further detected the gene expression involved in fibroblast migration using qRT-PCR (Fig. 9E–J). Compared with the blank group, the expression of six tested genes in the hydrogel group decreased, which was consistent with the result of the scratch test. The expression levels of a-SMA, Smad1, Smad8, and Rac in the hydrogel group with ES were higher than those in the hydrogel control group, indicating that the expression of a-SMA in fibroblasts was upregulated by the pulsed current stimulation. As cell migration involves cytoskeleton molecules such as actin and integrin, high level expression of a-SMA can be conducive to promoting cell migration, the activation of Smad signaling pathway can enhance the expression of stress fibers in fibroblasts and increases the contractility of cells [71], whereas Rac is the medium for lamellar foot protrusion that can promote cell movement [72]. Therefore, the faster closure rate observed in the H-30%IL-G3+ES group may be because of the upregulation of Smad1, Smad8, and Rac gene expression rather than hydrogel itself.

A full-thickness skin defect model in mice was used to evaluate the effect of hydrogel and electric stimulation on promoting wound healing (Fig. 10A). The results showed that the hydrogel group accelerated wound healing, compared with the gauze group, because in the process of wound repair, the humid hypoxic environment can maintain the normal electric potential gradient from the edge of the wound to the central, thus stimulating the formation of capillaries, whereas the hydrogel that contains a large amount of water can provide the local moist environment and its hydrophilic network can absorb the exudates of the wound, thereby promoting wound healing [75]. The wound healing rate of the hydrogel + ES group reached 94.0 ± 2.2% on the 15th day, the wound skin surface was smooth, and the hair distributed evenly. The healing rate of the hydrogel group was higher than that of the gauze group, and their healing rates were 83.7 ± 2.8% and 63.2 ± 4.3%, respectively (Fig. 10B). And then HE staining and Masson staining (Fig. 10C and D) were used to evaluate the histomorphology of the regenerated tissue. The results showed that the thickness of the epithelial layer of the hydrogel group was thicker than that of the control group, and the cuticle of the wound surface in the hydrogel + ES group was intact, and the basal keratinocytes of the wound surface in the hydrogel + ES group were arranged closely. The collagen content and granulation tissue thickness for the newly formed skin in the conductive gel group increased significantly, indicating that both wound healing rate and quality were promoted. Conductive hydrogel shows excellent wound repair performance, mainly because exogenous ES can help maintain or enhance endogenous wound current and promote cell migration to the wound by increasing the expression of migration-related genes, thereby inducing wound healing [76,77]. This is consistent with the results of in vitro cell experiments and also proves the important role of the conductivity of hydrogel in wound healing. In addition, compared with other groups, the degree of vascularization of the dermal tissue of the hydrogel + ES group was more significant. This indicates that ES can also promote angiogenesis by accelerating the wound healing through hydrogel, besides promoting the cell migration [78].

3.9. Hydrogel for the epidermal sensor

The high-reliability sensing ability of hydrogels for various strains originates from its good ionic conductivity, high mechanical strength, and good resilience. When strain is applied or eliminated, their electrical properties can respond quickly. In strain sensing test, it can be detected when the hydrogel changed from 0% strain to 400% strain, the brightness of the LED lamp connected to the circuit gradually decreased, showing a fast response to the strain (Video S1). In addition, the conductivity of the hydrogel could be affected by various deformations and was able to respond rapidly to them, indicating that it is a promising strain sensor material. Furthermore, we quantitatively investigated the effect of deformation on the conductivity of hydrogels (Fig. 11). The $\Delta R/R_0$ curves of hydrogels under different strains showed that during step-by-step stretch–holding process, the $\Delta R/R_0$ ratio increased step by step, and then during the gradual unloading–holding process, it decreased step by step. In addition, during the process of load-holding and unload-holding, the $\Delta R/R_0$ curves of the hydrogel showed stable platforms, and when the hydrogel completely unloaded stress, the ratio immediately returned to the original value, showing the excellent stability of electrical performance (Fig. 11B). To further investigate its electrical stability, it was subjected to several continuous load-unload cycles under 300% strain (Fig. 11C). It can be seen that the $\Delta R/R_0$ ratio could make an ultrafast response, and the relative resistance curve of each load-unload cycle was almost consistent, which indicates that it had excellent electrical stability and repeatability. When the applied cyclic tensile strain was 100%, 200%, 300%, and 400% (Fig. 11D), the relative resistance of the gel changed to varying degrees, and with the increase of tensile strain, the $\Delta R/R_0$ ratio increased, showing high strain sensitivity. In addition, the hydrogel could also respond rapidly to different strain rates with a tensile strain of 100%. From the variation of the $\Delta R/R_0$ curves of the hydrogel under different strains (Fig. 11E), it can be seen that the $\Delta R/R_0$ curves became sparse, with the decrease of the stretching frequency. As shown (Fig. 11F–H), the hydrogel strain sensor could directly adhere to the fingers without any adhesive tape to monitor the bending and tensile behavior of finger joints. The change of $\Delta R/R_0$ ratio could accurately reflect the bending of fingers at different angles. When the fingers were bent from 0 to 30°, 45°, and 90°, the $\Delta R/R_0$ ratio increased gradually. During the circulation, when the finger was bent at the same angle at any time, the $\Delta R/R_0$ ratio was consistent, showing good sensitivity and

Fig. 9. (A) Photos of material hemolysis assay. (B) Hemolysis ratio of the suspension of different hydrogels. Triton X-100 that induces significant hemolysis was used as the positive control, and PBS, which does not hemolyze erythrocytes, was used as the negative control. (C) Cell proliferation determined by means of the MTT assay at Days 1, 3, 5, and 7. The results were presented as the mean ± SD, and the experiments were performed in triplicate. (D) Images of the dual-fluorescence viability of the cells stained using AO/PI (all live nucleated cells fluoresce green and all dead nucleated cell ones red.), F-actin/DAPI (after cell culture for 5 days) and α-SMA (after cell culture for 7 days), all bars = 100 μm. Expression levels of (E) a-SMA, (F) Smad8, (G) Smad1, (H) Rac, (I) ID-1, and (J) Rho genes of fibroblasts for different experimental groups. The cells were harvested for gene expression analysis after AC voltage (5 V, 40 Hz) was applied through electrodes or the H-30%IL-G3 hydrogel for 1 h.

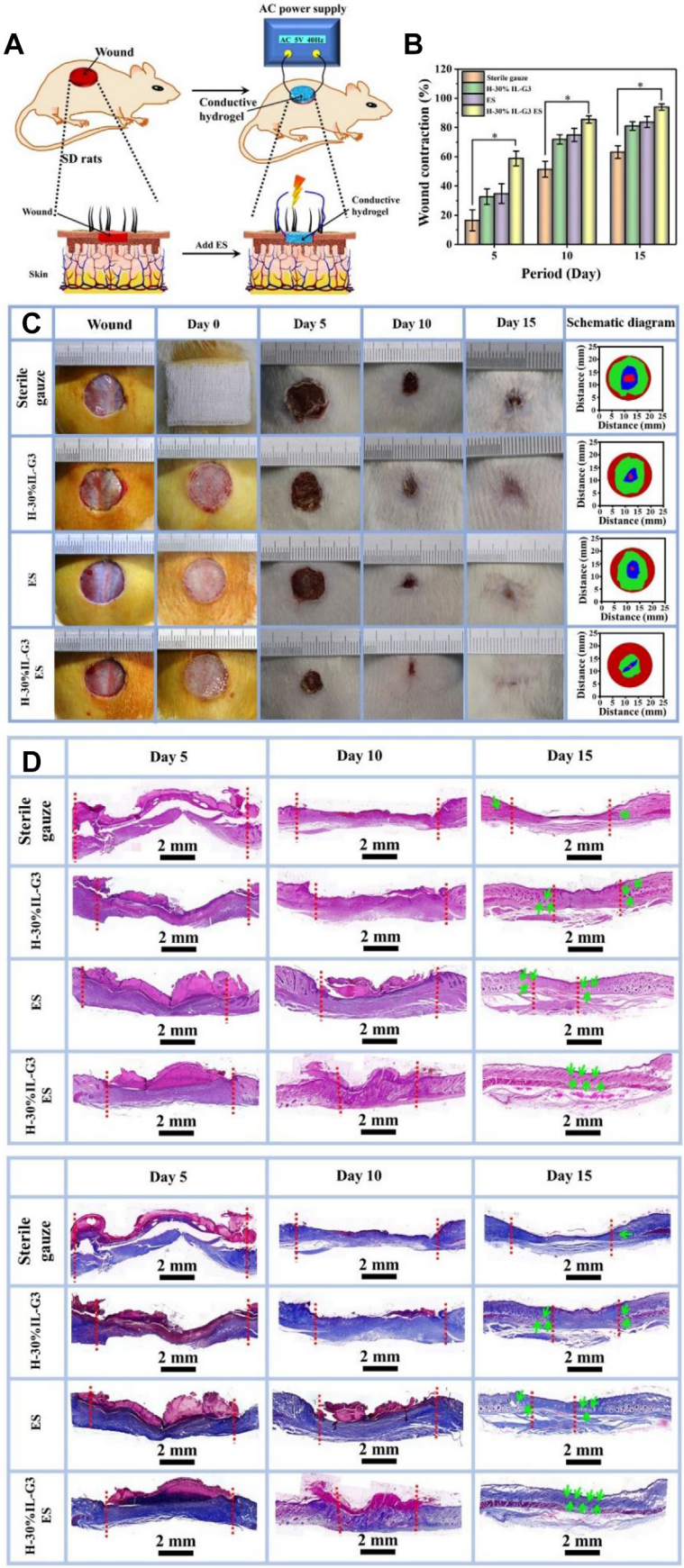

Fig. 10. (A) Scheme representation of the mouse wound repair. (B) Statistical contraction area of wounds (n = 5). (C) Photos and schematic diagram of the wound closure on the 5th, 10th, and 15th day. Histomorphological evaluation of the regenerated tissues by (D) H&E staining and (E) Masson's Trichrome staining.

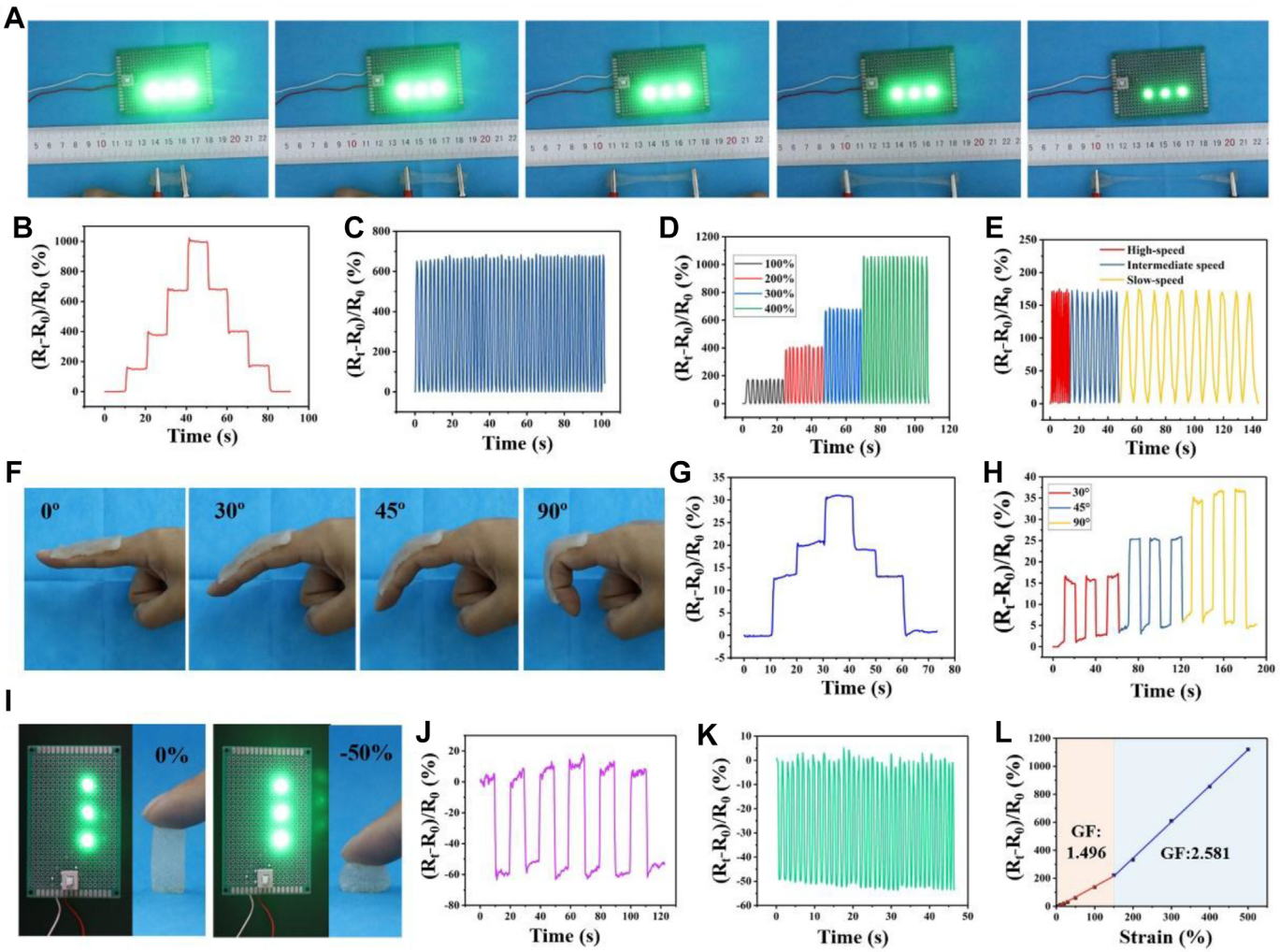

Fig. 11. (A) Photos of the brightness change of LED during the stretching of hydrogel connected in the electric circuit with LED. (B) Relative resistance change of the hydrogel during the gradual stretch–holding and unloading–holding process. (C) Consecutive cycle tests of the hydrogel at 300% stretch strain. (D) Cycle tests of the hydrogel at different loading–unloading strains. (E) Cycle tests of the hydrogel at different loading–unloading speeds. (F) Photos of finger bending at different angles (0°, 30°, 45°, and 90°) and (G) relative resistance changes of the hydrogel during the gradual bending–holding and unloading–holding process. (H) Cycle tests of the hydrogel at different finger bending angles. (I) Photos of the brightness change of LED for the compressed hydrogel connected in the electric circuit with LED. (J) Relative resistance change of the hydrogel during the gradual compress–holding and unloading–holding process. (K) Consecutive cycle tests of the hydrogel at 50% compress strain. (L) The relative resistance change and gauge factor under different strains. The relative resistance changes curves of hydrogel sensor at different tensile strains.

accuracy. Besides the strain sensing, the hydrogel also exhibited excellent pressure sensing properties (Fig. 11I–K). When a certain cyclic compressive stress was applied to the hydrogel, the relative resistance changed significantly- and had good reversibility and repeatability. After multiple loading–unloading cycles, the hydrogel still maintained good stability. Importantly, regardless of the strain or loading conditions of hydrogels, the $\Delta R/R_0$ ratio could change immediately, indicating that the hydrogel had not only excellent electrical stability and high strain sensitivity but also superfast response capability. GF was the ratio between the relative resistance variation and the applied strain, which is a common parameter to assess the sensitivity of the hydrogel sensors. As shown in Fig. 11(L), the curves for the relative resistance change in the tensile strain range of 0–500% were measured, and the corresponding GFs ($GF = (\Delta R/R0)/\varepsilon$) were also calculated to evaluate the electric sensitivity of the hydrogel. In the strain range of 0.5–150%, GF was 1.496, whereas in the strain range of 150–500%, GF was 2.581, which was the maximum value for the as-obtained conductive hydrogel, generally indicating that the as-obtained conductive hydrogel presented very high sensitivity. Thus, it can be used as a strain sensor to monitor human motion. We further investigated the effect of thickness on the resistance ratio for the samples with 5 cm in length and 1 cm in width but with variable thickness (Fig. S5). It was found that when the thickness of the samples increased from 0.2 cm to 1 cm, the resistance ratio decreased from 1.66 to 1.15, indicating that the thickness of the hydrogel had a great influence on the resistance ratio. The thinner the hydrogel, the higher the resistance ratio.

Supplementary data related to this article can be found at https://doi.org/10.1016/j.mtbio.2021.100138.

The strong adhesion between hydrogel sensors and human skin is very important for detecting and transmitting electrical signals under repeated deformation. The hydrogel that has good adhesion can be well adhered to the skin surface to detect the delicate dynamic process of human movement (Videos S2 and S3). In addition, we used conductive hydrogels to adhere to different joints (wrist, elbow, neck, and knee

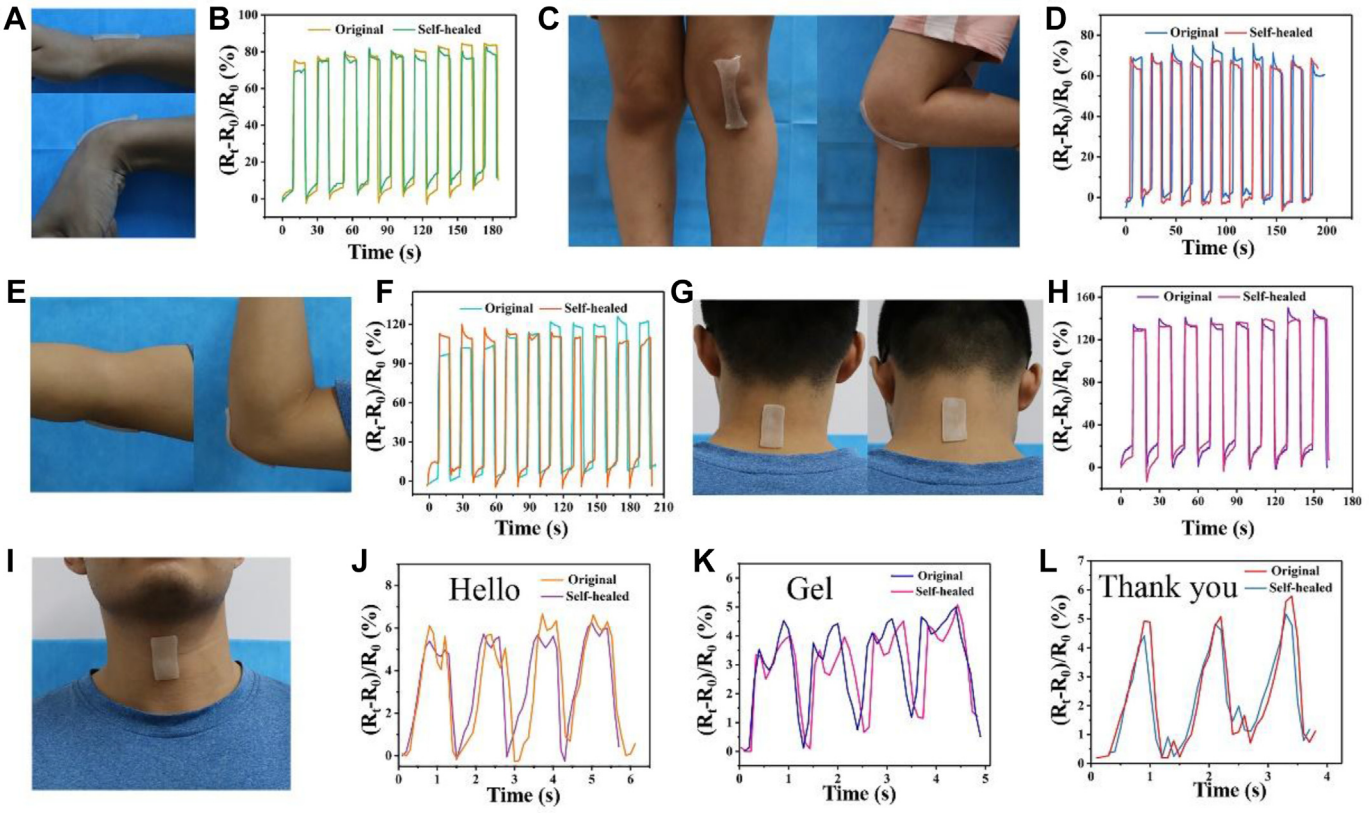

Fig. 12. Demonstration of the original and self-healed hydrogels as wearable strain sensors with strain sensitivity. The real-time detection of large-range human motions when the original and self-healed hydrogel strain sensors were directly adhered to (A, B) wrist, (C, D) knee joint, (E, F) elbow, and (G, H) neck. The real-time detection of slight-range human motions when the original and self-healed hydrogel strain sensors were directly adhered to (I) throat, and the curves of relative resistance changes when speaking the words (J) "Hello," (K) "Gel," and (L) "Thank you."

joints) to monitor big body movements (Fig. 12A–H). When the body is moving, different joints will bend to varying degrees. The hydrogel strain sensor will also be stretched to different degrees, thus causing the change of $\Delta R/R_0$ ratio. It can be seen that various bending behaviors of joints could be clearly identified because of the different deformation of hydrogel sensors under different joint movements; in addition, owing to the good recoverability of the hydrogel sensor, the baseline of relative resistance change has not changed significantly under repeated loading–unloading cycles. To further study, the potential of hydrogel, as a human motion sensor, adhered to the throat of volunteers to detect the strain sensitivity of slight physiological change when speaking (Fig. 12I-L). Before conducting the experiments, all volunteers were well informed about the experiments and agreed to participate. It could not only detect the change of real-time relative resistance when volunteers speak different words (such as Hello, thank you, and gel) but also showed significant reproducibility when repeating the same words and could distinguish these words according to different syllables. In general, the detected signal had high repeatability, regularity, and stability, indicating that such fast and accurate strain-sensitive conductive hydrogel sensor will provide great possibilities for wearable smart devices.

Supplementary data related to this article can be found at https://doi.org/10.1016/j.mtbio.2021.100138.

More importantly, benefiting from the excellent mechanical self-healing properties and electrical self-healing properties of hydrogels, the $\Delta R/R_0$ ratio of self-healing hydrogel has no obvious difference from the original hydrogel. The reproducibility was also maintained at the original level, indicating that its sensing properties have been fully recovered. Such hydrogel with good self-healing ability can reconstruct the complete mechanical and electrical network structure destroyed by repeated impact to restore its original sensing performance and to further enhance its stability, showing good application prospect.

4. Conclusions

We have successfully designed and prepared a mechanical, electrical dual self-healing multifunctional hydrogel. Dynamic radical reaction endowed the hydrogel with self-healing and antioxidant properties. By introducing imidazolium IL into the hydrogel system, the hydrogel was witnessed antibacterial and conductive properties. The addition of glycerol not only improved the mechanical and adhesive properties of the hydrogels but also gave the excellent antifreeze performance of the hydrogel so that it could work well even under extremely cold conditions. This multifunctional hydrogel that we have developed integrates conductivity, antibacterial, frost resistance, self-healing, adhesion, antioxidant, and biocompatibility in one. It can be used as wound dressing to promote wound healing and also can be used as a wearable strain sensor to achieve reliable application in health monitoring, human–machine interaction, and robotics. In the future, it might become a multipurpose material.

Credit author statement

Y.W. contributed to conceptualization, methodology, and writing and editing the article. Y.J. contributed to resources. H.R. contributed to visualization and investigation. C.L. contributed to investigation. W.P. contributed to resources. B.F. contributed to methodology. J.W. contributed to supervision, conceptualization, methodology, and reviewing the article.

Declaration of competing interest

The authors declare that they have no known competing financial interests or personal relationships that could have appeared to influence the work reported in this paper.

Acknowledgments

This work was supported by China's National Key Technology Research And Development Plan (2016YFC110200) and National Natural Science Foundation of China (No.51072167 and 31370966).

Appendix A. Supplementary data

Supplementary data to this article can be found online at https://doi.org/10.1016/j.mtbio.2021.100138.

References

[1] J. Bae, Y. Li, J. Zhang, X. Zhou, F. Zhao, Y. Shi, J.B. Goodenough, G. Yu, Titelbild: a 3D nanostructured hydrogel-framewor-derived high-performance composite polymer lithium-ion electrolyte, Angew. Chem. 57 (2018) 2096, https://doi.org/10.1002/ange.201800929.
[2] B. Zhang, J. He, M. Shi, Y. Liang, B. Guo, Injectable self-healing supramolecular hydrogels with conductivity and photo-thermal antibacterial activity to enhance complete skin regeneration, Chem. Eng. J. 400 (2020) 125994, https://doi.org/10.1016/j.cej.2020.125994.
[3] J. Zhang, C. Wu, Y. Xu, J. Chen, N. Ning, Z. Yang, Y. Guo, X. Hu, Y. Wang, ACS Appl. Mater. Interfaces 12 (2020) 40990.
[4] Q. Rong, W. Lei, J. Huang, M. Liu, Solar energy storage: liquid norbornadiene photoswitches for solar energy storage, Adv. Energy Mater. 8 (2018) 1801967, https://doi.org/10.1002/aenm.201870083.
[5] S. Zhang, S. Li, Z. Xia, K. Cai, J. Mater. Chem. B 8 (2020) 852.
[6] Y. Wang, Y. Yu, J. Guo, Z. Zhang, X. Zhang, Y. Zhao, Bio-inspired stretchable, adhesive, and conductive structural color film for visually flexible electronics, Adv. Funct. Mater. 30 (2020) 2000151, https://doi.org/10.1002/adfm.202000151.
[7] M. Li, Y. Liang, J. He, H. Zhang, B. Guo, Two-pronged strategy of biomechanically active and biochemically multifunctional hydrogel wound dressing to accelerate wound closure and wound healing, Chem. Mater. 32 (2020) 9937, https://doi.org/10.1021/acs.chemmater.0c02823.
[8] Z. Deng, H. Wang, P.X. Ma, B. Guo, Self-healing conductive hydrogels: preparation, properties and applications, Nanoscale 12 (2020) 1224, https://doi.org/10.1039/C9NR09283H.
[9] Z. Deng, R. Yu, B. Guo, Stimuli-responsive conductive hydrogels: design, properties, and applications, Mater. Chem. Front. 5 (2021) 2092, https://doi.org/10.1039/D0QM00868K.
[10] A. Sidorenko, T. Krupenkin, A. Taylor, P. Fratzl, J. Aizenberg, Reversible switching of hydrogel-actuated nanostructures into complex micropatterns, Science 315 (2007) 487, https://doi.org/10.1126/science.1135516.
[11] S. Maeda, Y. Hara, T. Sakai, R. Yoshida, S. Hashimoto, Self-walking gel, Adv. Mater. 19 (2007) 3480, https://doi.org/10.1002/adma.200700625.
[12] K. Imato, M. Nishihara, T. Kanehara, Y. Amamoto, A. Takahara, H. Otsuka, Self-healing of chemical gels cross-linked by diarylbibenzofuranone-based trigger-free dynamic covalent bonds at room temperature, Angew. Chem. Int. Ed. 51 (2012) 1138, https://doi.org/10.1002/anie.201104069.
[13] Z. Lei, H. Xiang, Y. Yuan, M. Rong, M. Zhang, Room-temperature self-healable and remoldable cross-linked polymer based on the dynamic exchange of disulfide bonds, Chem. Mater. 26 (2014) 2038–2046, https://doi.org/10.1021/cm4040616.
[14] B.G. Trewyn, C.M. Whitman, V.S.Y. Lin, Morphological control of room-temperature ionic liquid templated mesoporous silica nanoparticles for controlled release of antibacterial agents, Nano Lett. 4 (2004) 2139, https://doi.org/10.1021/nl048774r.
[15] X. Zhong, Z. Liu, D. Cao, Improved classical united-atom force field for imidazolium-based ionic liquids: tetrafluoroborate, hexafluorophosphate, methylsulfate, trifluoromethylsulfonate, acetate, trifluoroacetate, and bis(trifluoromethylsulfonyl)amide, J. Phys. Chem. B 115 (2011) 10027, https://doi.org/10.1021/jp204148q.
[16] Y. Danten, M.I. Cabaco, M. Besnard, et al., Interaction of water highly diluted in 1-Alkyl-3-methyl imidazolium ionic liquids with the PF6and BF4Anions, J. Phys. Chem. 113 (2009) 2873, https://doi.org/10.1021/jp8108368.
[17] P.C. Ray, A.K. Singh, D. Senapati, Z. Fan, H. Yu, J. Environ. Sci. Heal. C 27 (2009) 1.
[18] K. Murata, H. Tanaka, Nat. Mater. 11 (2012) 436.
[19] S. Zhu, J. Wang, H. Yan, Y. Wang, Y. Zhao, B. Feng, K. Duan, J. Weng, An injectable supramolecular self-healing bio-hydrogel with high stretchability, extensibility and ductility, and a high swelling ratio, J. Mater. Chem. B. 5 (2017) 7021–7034, https://doi.org/10.1039/C7TB01183K.
[20] C. Shen, P. Xu, B. Shen, H. Min, X. Li, J. Han, H. Yuan, Nanogel for dermal application of the triterpenoids isolated from Ganoderma lucidum (GLT) for frostbite treatment, Drug Deliv. 1 (2016) 610–618, https://doi.org/10.3109/10717544.2014.929756.
[21] M. Zilberman, D. Egozi, M. Shemesh, A. Keren, E. Mazor, M. Baranes-Zeevi, N. Goldstein, I. Berdicevsky, A. Gilhar, Y. Ullmann, Hybrid wound dressings with controlled release of antibiotics: structure-release profile effects and in vivo study in a Guinea pig burn model, Acta Biomater. 22 (2015) 155–163, https://doi.org/10.1016/j.actbio.2015.04.029.
[22] M.A. Zadeh, S. van der Zwaag, S.J. Garcia, Adhesion and long-term barrier restoration of intrinsic self-healing hybrid sol-gel coatings, J. ACS Appl. Mater. Interfaces 8 (2016) 4126, https://doi.org/10.1021/acsami.5b11867.
[23] C. Shao, L. Meng, M. Wang, C. Cui, B. Wang, C. Han, F. Xu, J. Yang, Mimicking dynamic adhesiveness and strain-stiffening behavior of biological tissues in tough and self-healable cellulose nanocomposite hydrogels, ACS Appl. Mater. Interfaces 11 (2019) 5885–5895, https://doi.org/10.1021/acsami.8b21588.
[24] Y. Lu, Y. Wang, J. Zhang, X. Hu, Z. Yang, Y. Guo, Y. Wang, In-situ doping of a conductive hydrogel with low protein absorption and bacterial adhesion for electrical stimulation of chronic wounds, Acta Biomater. 89 (2019) 217–226, https://doi.org/10.1016/j.actbio.2019.03.018.
[25] R. Ikeda, H. Tanaka, H. Uyama, S. Kobayashi, Enzymatic synthesis and curing of poly(cardanol), Polym. J. 32 (2000) 589–593, https://doi.org/10.1295/polymj.32.589.
[26] R. Ikeda, H. Tanaka, H. Uyama, S. Kobayashi, A new crosslinkable polyphenol from a renewable resource, Macromolecular Rapid Communications Macromol Rapid Commun 21 (2000) 496, https://doi.org/10.1002/(SICI)1521-3927(20000501)21:8<496::AID-MARC496>3.0.CO;2-G.
[27] X. Li, L. Liu, H. Bernhard Schlegel, On the physical origin of blue-shifted hydrogen bonds, J. Am. Chem. Soc. 124 (2002) 9639–9647, https://doi.org/10.1021/ja020213j.
[28] K. Imato, M. Nishihara, T. Kanehara, Y. Amamoto, A. Takahara, H. Otsuka, Self-healing of chemical gels cross-linked by diarylbibenzofuranone-based trigger-free dynamic covalent bonds at room temperature, Angew. Chem. Int. Ed. 124 (2012) 1164–1168, https://doi.org/10.1002/anie.201104069.
[29] Z. Zhao, Y. Liu, K. Zhang, S. Zhuo, R. Fang, J. Zhang, L. Jiang, M. Liu, Biphasic synergistic gel materials with switchable mechanics and self-healing capacity, Angew. Chem. Int. Ed. 129 (2017) 13464, https://doi.org/10.1002/ange.201707239.
[30] Y. Wang, Q. Xu, T. Chen, M. Li, B. Feng, J. Weng, K. Duan, W. Peng, J. Wang, A dynamic-coupling-reaction-based autonomous self-healing hydrogel with ultra-high stretching and adhesion properties, J. Mater. Chem. B. 7 (2019) 3044, https://doi.org/10.1039/C9TB00244H.
[31] Y. Shang, C. Wu, C. Hang, H. Lu, Q. Wang, Adv. Mater. 32 (2020) 2000189.
[32] X. He, C. Zhang, M. Wang, Y. Zhang, L. Liu, W. Yang, An electrically and mechanically autonomic self-healing hybrid hydrogel with tough and thermoplastic properties, ACS Appl. Mater. Interfaces 9 (2017) 11134, https://doi.org/10.1021/acsami.7b00358.
[33] M.A. Aboudzadeh, A.S. Shaplov, G. Hernandez, P.S. Vlasov, E.I. Lozinskaya, C. Pozo-Gonzalo, M. Forsyth, Y. Vygodskii, D. Mecerreyes, Supramolecular ionic networks with superior thermal and transport properties based on novel delocalized di-anionic compounds, J. Mater. Chem. 3 (2015) 2338–2343, https://doi.org/10.1039/C4TA05792A.
[34] C.-J. Lee, H. Wu, Y. Hu, M. Young, H. Wang, D. Lynch, F. Xu, H. Cong, G. Cheng, Ionic conductivity of polyelectrolyte hydrogels, ACS Appl. Mater. Interfaces 10 (2018) 5845, https://doi.org/10.1021/acsami.7b15934.
[35] J. Huang, P.F. Miller, J.S. Wilson, A.J. Mello, J.C. Mello, D.D.C. Bradley, Adv. Funct. Mater. 15 (2005) 290.
[36] X. Zhong, Z. Fan, Z. Liu, D. Cao, Local structure evolution and its connection to thermodynamic and transport properties of 1-Butyl-3-methylimidazolium tetrafluoroborate and water mixtures by molecular dynamics simulations, J. Phys. Chem. B 116 (2012) 3249, https://doi.org/10.1021/jp3001543.
[37] Y. Jian, S. Handschuh-Wang, J. Zhang, W. Lu, X. Zhou, T. Chen, Correction: biomimetic anti-freezing polymeric hydrogels: keeping soft-wet materials active in cold environments, Mater. Horiz. (2020), https://doi.org/10.1039/D0MH90071K.
[38] A.A. Zavitsas, Properties of water solutions of electrolytes and nonelectrolytes, J. Phys. Chem. B 105 (2001) 7805–7817, https://doi.org/10.1021/jp011053l.
[39] F. Chen, D. Zhou, J.H. Wang, T.Z. Li, X.H. Zhou, T.S. Gan, S.H. Wang, X.C. Zhou, Angew. Chem. Int. Ed. 57 (2018) 6568.
[40] Q.F. Rong, W.W. Lei, L. Chen, Y.A. Yin, J.J. Zhou, M.J. Liu, Angew. Chem. Int. Ed. 56 (2017) 14159.
[41] J.H. Liu, C.M. Xie, A. Kretzschmann, K. Koynow, H.J. Butt, S. Wu, Metallopolymer organohydrogels with Photo✕ontrolled coordination crosslinks work properly below 0 °C, Adv. Mater. (2020) 1908324, https://doi.org/10.1002/adma.201908324.
[42] M. Ju, B.H. Wu, S.T. Sun, P.Y. Wu, Adv. Funct. Mater. (2020) 1910387.
[43] H. Liu, W. Zhao, G.H. Gao, X.Y. Ren, Mater. Today Commun. 21 (2019) 100609.
[44] X. Zhang, C. Bai, Y. Zhang, H. Wu, Can. J. Chem. 82 (2004) 616.
[45] Q. Rong, W. Lei, L. Chen, Y. Yin, J. Zhou, M. Liu, Anti-freezing, conductive self-healing organohydrogels with stable strain-sensitivity at subzero temperatures, Angew. Chem. Int. Ed. 56 (2017) 14159–14163, https://doi.org/10.1002/ange.201708614.
[46] W.P. Williams, P. J Quinn, L.I. Tsonev, R.D. Koynova, The effects of glycerol on the phase behaviour of hydrated distearoylphosphatidylethanolamine and its possible relation to the mode of action of cryoprotectants, Biochim. Biophys. Acta 1062 (1991) 123–132, https://doi.org/10.1016/0005-2736(91)90383-J.
[47] C. Shen, P. Xu, B. Shen, H. Min, X. Li, J. Han, H. Yuan, Nanogel for dermal application of the triterpenoids isolated from Ganoderma lucidum (GLT) for frostbite treatment, Drug Deliv. 1 (2015), https://doi.org/10.3109/10717544.2014.929756.
[48] F. Pu, X. Liu, B. Xu, J. Ren, X. Qu, Miniaturization of metal–biomolecule frameworks based on stereoselective self-assembly and potential application in water treatment and as antibacterial agents, Chem. Eur J. 18 (2012) 4322, https://doi.org/10.1002/chem.201103524.
[49] P. Li, C. Zhou, S. Rayatpisheh, K. Ye, Y.F. Poon, P.T. Hammond, H. Duan, M.B. Chan-Park, Cationic peptidopolysaccharides show excellent broad-spectrum antimicrobial activities and high selectivity, Adv. Mater. 24 (2012) 4130–4137, https://doi.org/10.1002/adma.201104186.
[50] M. Li, J. Chen, M. Shi, H. Zhang, P.X. Ma, B. Guo, Electroactive anti-oxidant polyurethane elastomers with shape memory property as non-adherent wound

dressing to enhance wound healing, Chem. Eng. J. 375 (2019) 121999, https://doi.org/10.1016/j.cej.2019.121999.
[51] X. Zhao, H. Wu, B. Guo, R. Dong, Y. Qiu, P.X. Ma, Antibacterial anti-oxidant electroactive injectable hydrogel as self-healing wound dressing with hemostasis and adhesiveness for cutaneous wound healing, Biomaterials 122 (2017) 34–47, https://doi.org/10.1016/j.biomaterials.2017.01.011.
[52] J. Qu, X. Zhao, Y. Liang, Y. Xu, P.X. Ma, B. Guo, Chem. Eng. J. 362 (2019) 548.
[53] T.A. Barhé, G.R.F. Tchouya, Arabian J. Chem. 9 (2016) 1.
[54] J. Wang, L. Tian, B. Luo, S. Ramakrishn, D. Kai, X.J. Loh, I.H. Yang, G.R. Deen, X. Mo, Colloids Surf., B 169 (2018) 356.
[55] F. Chen, M. Zhang, Maleic anhydride-modified polyolefins as compatibilizer for lignin-reinforced polypropylene composites, Polym. Compos. 7 (2018) 2594–2601, https://doi.org/10.1002/pc.25053.
[56] H. Cui, Y. Liu, Y. Cheng, Z. Zhang, P. Zhang, X. Chen, Y. Wei, In vitro study of electroactive tetraaniline-containing thermosensitive hydrogels for cardiac tissue engineering, Biomacromolecules 15 (2014) 1115–1123, https://doi.org/10.1021/bm4018963.
[57] C. Gong, Q. Wu, Y. Wang, D. Zhang, F. Luo, X. Zhao, Y. Wei, Z. Qian, Biomaterials 34 (2013) 6377.
[58] R. Moseley, M. Walker, R.J. Waddington, W. Chen, Comparison of the antioxidant properties of wound dressing materials–carboxymethylcellulose, hyaluronan benzyl ester and hyaluronan, towards polymorphonuclear leukocyte-derived reactive oxygen species, Biomaterials 24 (2003), https://doi.org/10.1016/S0142-9612(02)00540-9, 1549-155.
[59] C.Y. Wang, F. Huang, X. Chen, X. Wang, W. Zhang, J. Peng, J. Li, M. Zhai, Stretchable, conductive and self-healing hydrogel with super metal adhesion, Chem. Mater. 30 (2018) 4289. https://do.org/10.1021/acs.chemmater.8b01260.
[60] T.T.H. Thi, J.S. Lee, Y. Lee, H.B. Park, K.M. Park, K.D. Park, Supramolecular cyclodextrin supplements to improve the tissue adhesion strength of gelatin bioglues, ACS Macro Lett. 6 (2017) 83–88, https://doi.org/10.1021/acsmacrolett.6b00841.
[61] M. Shan, C. Gong, B. Li, G. Wu, Polym. Chem. 8 (2017) 2997.
[62] A.G. Lyapin, E.L. Gromnitskaya, I.V. Danilov, V.V. Brazhkina, Elastic properties of the hydrogen-bonded liquid and glassy glycerol under high pressure: comparison with propylene carbonate, RSC Adv. 7 (2017) 33278–33284, https://doi.org/10.1039/C7RA06165J.
[63] J. Shin, J.S. Lee, C. Lee, H.J. Park, K. Yang, Y. Jin, J.H. Ryu, K.S. Hong, S.H. Moon, H.M. Chung, Adv. Funct. Mater. 25 (2015) 3814.
[64] R. Wang, J. Li, W. Chen, T. Xu, S. Yun, Z. Xu, Z. Xu, T. Sato, B. Chi, H. Xu, A biomimetic mussel-inspired ε-Poly-l-lysine hydrogel with robust tissue-anchor and anti-infection capacity, Adv. Funct. Mater. 27 (2017) 1604894, https://doi.org/10.1002/adfm.201604894.
[65] J. Xu, Z. Fan, L. Duan, G. Gao, Polym. Chem. 9 (2018) 2617.
[66] L. Han, K. Liu, M. Wang, K. Wang, L. Fang, H. Chen, J. Zhou, X. Lu, Mussel-inspired adhesive and conductive hydrogel with long-lasting moisture and extreme temperature tolerance, Adv. Funct. Mater. 28 (2018) 1704195, https://doi.org/10.1002/adfm.201704195.
[67] K. Yang, J.S. Lee, J. Kim, Y.B. Lee, H. Shin, S.H. Um, J.B. Kim, K.I. Park, H. Lee, S.W. Cho, Corrigendum to "Polydopamine-mediated surface modification of scaffold materials for human neural stem cell engineering, Biomaterials 33 (2012) 6952–6964, https://doi.org/10.1016/j.biomaterials.2012.08.001.
[68] L.C. Kloth, 5 questions–and answers–about electrical stimulation, Adv. Skin Wound Care 14 (2001) 156, https://doi.org/10.1097/00129334-200105000-00017.
[69] L. Han, K. Liu, M. Wang, K. Wang, L. Fang, H. Chen, J. Zhou, X. Lu, Adv. Funct. Mater. 28 (2018) 1704195.
[70] L.C. Kloth, 5 questions–and answers–about electrical stimulation, Adv. Skin Wound Care 14 (2001) 156. https://scite.ai/reports/10.1097/00129334-200105000-00017.
[71] L. Wang, G. Gao, Y. Zhou, T. Xu, J. Chen, R. Wang, R. Zhang, J. Fu, Tough, adhesive, self-healable, and transparent ionically conductive zwitterionic nanocomposite hydrogels as skin strain sensors, ACS Appl. Mater. Interfaces 11 (2019) 3506, https://doi.org/10.1021/acsami.8b20755.
[72] L. Wang, Y. Wu, T. Hu, B. Guo, P.X. Ma, Electrospun conductive nanofibrous scaffolds for engineering cardiac tissue and 3D bioactuators, Acta Biomater. 59 (2017) 68, https://doi.org/10.1016/j.actbio.2017.06.036.
[73] X. Xu, P. Fan, J. Ren, Y. Cheng, J. Ren, J. Zhao, R. Song, Compos. Sci. Technol. 168 (2018) 255.
[74] X. Zhao, B. Guo, H. Wu, Y. Liang, P.X. Ma, Injectable antibacterial conductive nanocomposite cryogels with rapid shape recovery for noncompressible hemorrhage and wound healing, Nat. Commun. 9 (2018) 2784, https://doi.org/10.1038/s41467-018-04998-9.
[75] Z. Fan, B. Liu, J. Wang, S. Zhang, Q. Lin, P. Gong, L. Ma, S. Yang, A novel wound dressing based on Ag/graphene polymer hydrogel: effectively kill bacteria and accelerate wound healing, Adv. Funct. Mater. 24 (2014) 3933, https://doi.org/10.1002/adfm.201304202|.
[76] M. Rouabhia, H. Park, S. Meng, H. Derbali, Z. Zhang, Electrical stimulation promotes wound healing by enhancing dermal fibroblast activity and promoting myofibroblast transdifferentiation, PloS One 8 (2013), e71660, https://doi.org/10.1371/journal.pone.0071660.
[77] M. Ashrafi, T. Alonso-Rasgado, M. Baguneid, A. Bayat, The efficacy of electrical stimulation in lower extremity cutaneous wound healing: a systematic review, Exp. Dermatol. 26 (2017) 171, https://doi.org/10.1111/exd.13179.
[78] Y. Hu, S. Rao, Z. Wang, J. Cao, Y. Tan, J. Luo, H. Li, W. Zhang, C. Chen, H. Xie, Exosomes from human umbilical cord blood accelerate cutaneous wound healing through miR-21-3p-mediated promotion of angiogenesis and fibroblast function, Theranostics 8 (2018) 169–184, https://doi.org/10.7150/thno.21234.